



# FLEXEVENT: EVENT CAMERA OBJECT DETECTION AT ARBITRARY FREQUENCIES

Dongyue Lu<sup>1</sup>, Lingdong Kong<sup>1</sup>, Gim Hee Lee<sup>1</sup>, Camille Simon Chane<sup>2</sup>, Wei Tsang Ooi<sup>1</sup>

<sup>1</sup>National University of Singapore

<sup>2</sup>Ecole Nationale Supérieure de l'Electronique et de ses Applications

dongyue.lu@u.nus.edu {lingdong, ooiwt}@comp.nus.edu.sg

camille.simon-chane@ensea.fr gimhee.lee@nus.edu.sg

<https://flexevent.github.io>

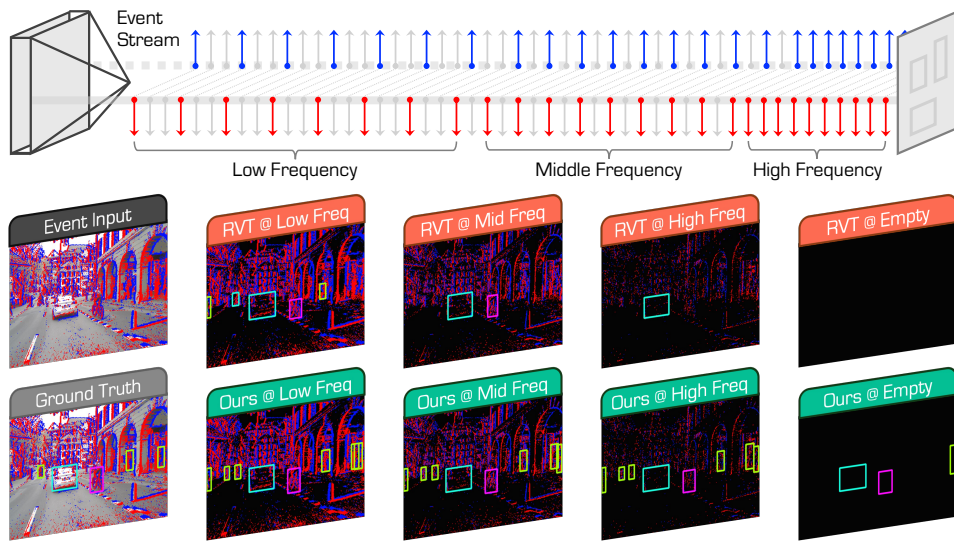


Figure 1: **Event camera detection at varying frequencies.** The performance of the classic RVT detector (Gehrig & Scaramuzza, 2023) drops significantly at higher event operational frequencies. Motivated by this, we propose **FlexEvent**, a robust and flexible detector that maintain high accuracy across a wide range of frequencies, ensuring strong adaptability in dynamic sensing environments.

## ABSTRACT

Event cameras offer unparalleled advantages for real-time perception in dynamic environments, thanks to their microsecond-level temporal resolution and asynchronous operation. Existing event-based object detection methods, however, are limited by fixed-frequency paradigms and fail to fully exploit the high-temporal resolution and adaptability of event cameras. To address these limitations, we propose **FlexEvent**, a novel event camera object detection framework that enables detection at arbitrary frequencies. FlexEvent consists of two key components: **FlexFuser**, an adaptive event-frame fusion module that integrates high-frequency event data with rich semantic information from RGB frames, and **FAL**, a frequency-adaptive learning mechanism that generates frequency-adjusted labels to enhance model generalization across varying operational frequencies. This combination allows FlexEvent to detect objects with high accuracy in both fast-moving and static scenarios, while adapting to dynamic environments. Extensive experiments on large-scale event camera datasets demonstrate that our approach surpasses state-of-the-art methods, achieving significant improvements in both standard and high-frequency settings. Notably, FlexEvent maintains robust performance when scaling from 20 Hz to 90 Hz and delivers accurate detection up to 180 Hz, proving its effectiveness in extreme conditions. Our framework sets a new benchmark for event-based object detection and paves the way for more adaptable, real-time vision systems. The code will be made publicly available to facilitate future research.

## 1 INTRODUCTION

Event cameras have garnered significant attention for their ability to capture dynamic scenes with microsecond-level temporal resolution (Gallego et al., 2022). Unlike conventional RGB cameras, which capture entire frames at fixed intervals, event cameras operate asynchronously, responding to changes in pixel intensity at each location (Zou et al., 2022). This low-latency operation reduces motion blur and enables highly energy-efficient sensing, making event cameras ideal for real-time applications such as autonomous driving, robotics, and surveillance (Steffen et al., 2019).

Despite their potential, existing event camera object detection methods often fail to fully leverage the high-frequency temporal information captured by event cameras (Cordone et al., 2022; Gehrig & Scaramuzza, 2022; Jeziorek et al., 2023). Most approaches align event data with the lower frequency of RGB cameras by adopting a fixed time interval between event streams and frame-based annotations (Perot et al., 2020; Gehrig et al., 2021b). While this strategy simplifies data processing, it inevitably overlooks the rich temporal details embedded in high-frequency event streams. Given that human annotations are often synchronized with slower frame rates, current detection models miss valuable information from high-frequency event data, resulting in suboptimal performance when rapid object detection is required in dynamic environments (Messikommer et al., 2020; Schaefer et al., 2022).

To address these limitations, we introduce **FlexEvent**, a novel event camera object detection framework designed to tackle the challenging problem of object detection at varying operational frequencies. Our approach addresses the need for high-frequency detection in fast-changing environments, while adapting to different operational frequencies. We propose two key innovations: (1) **FlexFuser**, an adaptive event-frame fusion module, and (2) **FAL**, a frequency-adaptive learning mechanism.

**Flexible Event-Frame Fusion.** The first component, FlexFuser, addresses the limitations of event data, which often lacks semantic and texture-rich information, especially at higher frequencies (Zhou et al., 2023), by integrating the rich spatial and semantic information from RGB frames with the high-temporal resolution of event streams. It enables high detection accuracy even in fast-moving environments. Furthermore, training on high-frequency event data is computationally expensive and impractical due to the significant human effort required to label such data. FlexFuser mitigates this by sampling event data at varying frequencies, aligning them with the normal frame rate during training, thus maintaining efficiency while preserving the high-frequency benefits at inference time.

**Frequency-Adaptive Learning.** The second component, FAL, enhances the generalization capability of event camera detectors across varying operational frequencies, by generating frequency-adaptive labels for the unlabeled high-frequency data. These labels allow the model to learn from high-frequency event streams without manual annotations, and iterative refinement through self-training ensures that the model remains robust across different motion dynamics and frequency settings. Together, these two components allow for accurate real-time detection in rapid scene changes and adapt to a wide range of operational frequencies, by leveraging the temporal richness of event data and the semantic detail of RGB frames.

Our extensive experiments validate the effectiveness of **FlexEvent** on multiple large-scale event camera datasets. Our approach consistently outperforms recent detectors across both standard and high-frequency settings. In particular, we achieve mAP gains of 15.5%, 9.4%, and 10.3% over the previous best-performing detectors on the *DSEC-Det* (Gehrig & Scaramuzza, 2024), *DSEC-Detection* (Tomy et al., 2022), and *DSEC-MOD* (Zhou et al., 2023) datasets, respectively. Our model also maintains 96.2% of its performance when the operational frequency shifts from 20 Hz to 90 Hz, and delivers accurate detection at frequencies as high as 180 Hz, proving its robustness under extreme conditions.

In summary, our contributions are listed as follows:

- ▶ The **FlexEvent** framework is designed to tackle the challenging problem of event camera object detection at arbitrary frequencies, being one of the first works to address this problem explicitly.
- ▶ We propose FlexFuser, an adaptive event-frame fusion that leverages the strengths of both event and frame data, enabling efficient and accurate detection in dynamic environments.
- ▶ We introduce FAL, a frequency-adaptive learning mechanism that generates frequency-adaptive labels and improves generalization across a wide range of motion frequencies.

- We demonstrate that our approach achieves state-of-the-art performance in event-based object detection across large-scale datasets, particularly in high-frequency scenarios, validating its effectiveness and potential to handle safety-critical problems in the real world.

## 2 RELATED WORK

**Event Camera Object Detection.** Event-based detection methods can be broadly split into two approaches: GNNs/SNNs and dense feed-forward models. GNNs build dynamic spatio-temporal graphs by subsampling events (Gehrig & Scaramuzza, 2022; Sun & Ji, 2023; Messikommer et al., 2020; Schaefer et al., 2022), but they face challenges in propagating information over large spatio-temporal regions, especially for slow-moving objects. SNNs offer efficient sparse information transmission but are often hindered by their non-differentiable nature, complicating optimization processes (Cuadrado et al., 2023; Cordone et al., 2022; Zhang et al., 2022). Dense, feed-forward models represent the second approach. Initial methods using fixed temporal windows (Chen, 2018; Iacono et al., 2018; Jiang et al., 2019) struggle with slow-moving or stationary objects due to their limited capability to capture long-term temporal data. Subsequent advancements incorporate RNNs and transformers to enhance temporal modeling capabilities (Perot et al., 2020; Zubić et al., 2023; Li et al., 2022; Gehrig & Scaramuzza, 2023; Peng et al., 2024), but these models often still lack semantic richness and face difficulties in adapting to variable frequencies and highly dynamic scenarios.

**Event-Frame Multimodal Learning.** To overcome the limited texture in event streams, multimodal fusion techniques combining event-based and frame-based data have gained traction across tasks, such as deblurring (Sun et al., 2022a; Zhang et al., 2020), depth estimation (Gehrig et al., 2021a; Uddin et al., 2022), and tracking (Zhao et al., 2022; Gehrig et al., 2020). Earlier object detection approaches fuse event and image data during post-processing (Li et al., 2019; Chen et al., 2019), but they lack meaningful feature-level interaction. Recent works focus on deeper feature fusion (Tomy et al., 2022; Cao et al., 2022; 2021), with advanced methods introducing pixel-level spatial attention or temporal transformers for asynchronous processing (Zhou et al., 2023; Li et al., 2023; Gehrig & Scaramuzza, 2024; Cao et al., 2024). Some approaches (Li et al., 2023; Gehrig et al., 2021a) explore combining events and frames through asynchronous multi-modal fusion, enabling inference at varying frequencies. However, they do not focus on high-frequency event data and fully leverage the temporally rich nature of event streams. Furthermore, these methods still face challenges in fully exploiting complementary strengths and addressing feature imbalance in event-frame detection. Unlike previous methods, **FlexEvent** employs a more comprehensive fusion framework that effectively combines high-temporal resolution event data with rich semantics from RGB frames, enabling robust object detection across varying frequencies while addressing feature imbalance.

**Label-Efficient Learning in Event Data.** Due to limited annotated datasets, label-efficient learning has become an important area for event-based vision. Several studies attempt to reconstruct images from event data (Rebecq et al., 2019; 2021; Stoffregen et al., 2020) or leverage knowledge distillation from pre-trained frame-based models (Wang et al., 2021; Sun et al., 2022b; Yang et al., 2023; Kong et al., 2024). Other approaches utilize pre-trained models or self-supervised losses (Klenk et al., 2022; Wu et al., 2023; Zhu et al., 2019). LEOD (Wu et al., 2024) pioneers object detection with limited labels but does not address high-frequency generalization. A recent state-space model (Zubić et al., 2024) adapts to varying frequencies without retraining but struggles to detect static objects at high frequencies due to its reliance solely on event data. In contrast, **FlexEvent** is specifically designed to adapt to varying event frequencies, ensuring consistent performance even in scenarios with limited labels, and effectively detecting both stationary and fast-moving objects.

## 3 FLEXEVENT: A FLEXIBLE EVENT OBJECT DETECTOR

In this section, we elaborate on the technical details of our **FlexEvent** framework. We start with the foundational concepts of event data and their representation in Sec. 3.1. We then introduce the **FlexFuser** module in Sec. 3.2, which adaptively fuses event and frame data to enhance detection across varying frequencies. Finally, we detail the frequency-adaptive learning (**FAL**) mechanism in Sec. 3.3, which enables our model to generalize effectively across diverse temporal conditions using self-training and adaptive label generation. The overall framework is illustrated in Fig.2.

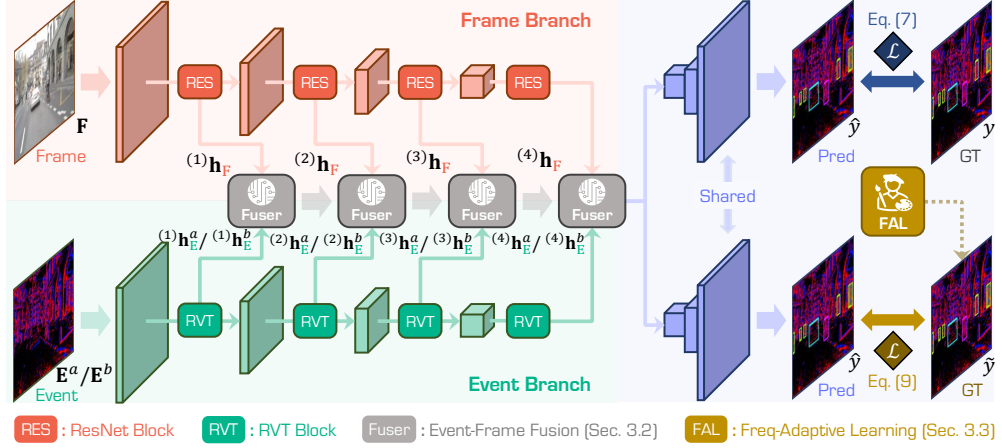


**Figure 2: Framework Overview.** The proposed **FlexEvent** consists of two branches: **Event** and **Frame**. The event branch captures high-temporal resolution data, while the frame branch leverages the rich semantic information from frames (*cf.* Sec. 3.1). These branches are fused dynamically through **FlexFuser**, allowing adaptive integration of event and frame data (*cf.* Sec. 3.2). Additionally, the frequency-adaptive learning (**FAL**) mechanism ensures robust detection performance across varying operational frequencies (*cf.* Sec. 3.3). Together, these components enable the model to handle diverse motion dynamics and maintain high detection accuracy in varying frequency scenarios.

### 3.1 BACKGROUND & PRELIMINARIES

**Event Processing.** Event cameras are bio-inspired vision sensors that capture changes in log intensity per pixel asynchronously, rather than capturing entire frames at fixed intervals. Formally, let  $I(x, y, t)$  denote the log intensity at pixel coordinates  $(x, y)$  and time  $t$ . An event  $e$  is generated at  $(x, y, t)$  whenever the change in log intensity  $\Delta I$  exceeds a certain threshold  $C$ . Such a process can be modeled as:

$$\Delta I(x, y, t) = I(x, y, t) - I(x, y, t - \Delta t) \geq C. \quad (1)$$

Each event  $e$  is a tuple  $(x, y, t, p)$ , where  $(x, y)$  are the pixel coordinates,  $t$  is the timestamp, and  $p \in \{-1, 1\}$  denotes the polarity of the event which indicates the direction of the intensity change.

To leverage event data with convolutional neural network layers, we preprocess events into a 4D tensor  $E$  with dimensions representing the polarity, temporal discretization  $T$ , and spatial dimensions  $(H, W)$ . This representation involves mapping a set of events  $\mathcal{E}$  within time interval  $[t_a, t_b]$  into:

$$E(p, \tau, x, y) = \sum_{e_k \in \mathcal{E}} \delta(p - p_k) \delta(x - x_k, y - y_k) \delta(\tau - \tau_k), \quad (2)$$

where  $\tau_k = \left\lfloor \frac{t_k - t_a}{t_b - t_a} \cdot T \right\rfloor$ . This tensor captures event activity in  $T$  discrete time slices, yielding a compact representation suitable for 2D convolutions by flattening the polarity and temporal dimensions.

**Problem Formulation.** Given two consecutive frames  $F_a$  and  $F_b$  captured at timestamps  $T_a$  and  $T_b$ , our objective is to leverage the event stream over the interval  $[T_a, T_b]$  to detect objects at the end timestamp  $T_b$ . Existing event-based object detection methods often use fixed time intervals  $\Delta T$ , limiting adaptability to dynamic environments (Perot et al., 2020). Additionally, integrating semantic information from RGB frames remains challenging, affecting performance in complex scenarios (De Tournemire et al., 2020). To address this, we synchronize event data with frames and explore varying training frequencies, leveraging the temporal richness of event cameras to improve detection accuracy.

### 3.2 FLEXFUSER: AN ADAPTIVE EVENT-FRAME FUSION MODULE

In dynamic environments, object detection systems must adapt to varying motion frequencies (Sun et al., 2022a). While event cameras excel at capturing rapid changes in pixel intensity, they often lack the rich spatial and semantic information provided by frames. To address this limitation and

fully leverage the complementary strengths of both modalities, we introduce **FlexFuser**, an adaptive fusion module designed to dynamically combine event data at different frequencies with frame data.

**Dynamic Event Aggregation.** Given a dataset  $\mathcal{D}$ , consisting of sequences of calibrated event camera data and frame data with a resolution of  $H \times W$ , along with corresponding bounding box annotations  $y$  collected at frequency  $a$ , we begin by selecting a batch of frame data  $\mathbf{F}$  paired with event data  $\mathbf{E}^a$ , both captured at frequency  $a$ . To aggregate event data from a higher frequency  $b$  (where  $b > a$ ), we divide the time interval  $\Delta T^a$  corresponding to  $\mathbf{E}^a$  into  $b/a$  smaller sub-intervals. From each sub-interval, we obtain a high-frequency event set  $\{\mathbf{E}_i^b\}_{i=0}^{b/a}$ , as defined in Eq. 2. From this set, we randomly sample one event data point<sup>1</sup>  $\mathbf{E}^b$ . By doing so, the sampled high-frequency event data  $\mathbf{E}^b$  is temporally aligned with the frame data  $\mathbf{F}$  and the base frequency event data  $\mathbf{E}^a$ . This synchronization of event streams at different frequencies ensures consistent and reliable processing for subsequent stages.

**Feature Extraction.** Let  $\phi_{\mathbf{E}}(\cdot)$  and  $\phi_{\mathbf{F}}(\cdot)$  represent the event- and frame-based networks, respectively, where the former employs the RVT (Gehrig & Scaramuzza, 2023) for extracting features from event data, and the latter uses ResNet-50 (He et al., 2016) for feature extraction from frames. Both networks are structured into four stages, as shown in Fig. 2.

At each scale  $i$ , we extract features  $(i)\mathbf{h}_{\mathbf{E}}^a, (i)\mathbf{h}_{\mathbf{E}}^b$  from the event data and  $(i)\mathbf{h}_{\mathbf{F}}$  from the frame data:

$$(i)\mathbf{h}_{\mathbf{E}}^a = \phi_{\mathbf{E}}^{(i)}(\mathbf{E}^a), \quad (i)\mathbf{h}_{\mathbf{E}}^b = \phi_{\mathbf{E}}^{(i)}(\mathbf{E}^b), \quad (i)\mathbf{h}_{\mathbf{F}} = \phi_{\mathbf{F}}^{(i)}(\mathbf{F}), \quad (3)$$

where  $(i)\mathbf{h}_{\mathbf{E}}^a$  and  $(i)\mathbf{h}_{\mathbf{E}}^b \in \mathbb{R}^{B \times C_{\mathbf{E}} \times H_i \times W_i}$ ,  $(i)\mathbf{h}_{\mathbf{F}} \in \mathbb{R}^{B \times C_{\mathbf{F}} \times H_i \times W_i}$ . Here,  $i$  denotes the scale,  $B$  is the batch size, and  $C_{\mathbf{E}}$  and  $C_{\mathbf{F}}$  are the dimensions of the feature maps extracted from the event and frame data, respectively.

**Event-Frame Adaptive Fuser.** To effectively fuse the event and frame data, we employ an adaptive fuser that is consistent across different event data frequencies. At each scale  $i$ , taking the low-frequency event features  $(i)\mathbf{h}_{\mathbf{E}}^a$  as an example, we concatenate the feature maps from both the event and frame branches as follows:

$$(i)\mathbf{h}_{\text{shared}}^a = \left[ (i)\mathbf{h}_{\mathbf{E}}^a, (i)\mathbf{h}_{\mathbf{F}} \right] \in \mathbb{R}^{B \times (C_{\mathbf{E}} + C_{\mathbf{F}}) \times H_i \times W_i}. \quad (4)$$

Inspired by previous works (Zhou et al., 2023) and (Zhong et al., 2024), our goal is to dynamically fuse these two modalities in a flexible manner. The proposed FlexFuser module computes adaptive soft weights that regulate the contribution of each branch (event and frame) based on the current input conditions. As shown in Fig. 3, these adaptive soft weights are computed using a gating function, which incorporates learned noise to introduce perturbations for improved adaptability. The process is:

$$\begin{bmatrix} (i)\boldsymbol{\alpha}, (i)\boldsymbol{\beta} \end{bmatrix} = \text{Softmax} \left( ((i)\mathbf{h}_{\text{shared}}^a \cdot (i)\mathbf{W}) + (i)\sigma \cdot \epsilon \right), \quad (5)$$

where  $(i)\mathbf{W} \in \mathbb{R}^{(C_{\mathbf{E}} + C_{\mathbf{F}}) \times 2}$  is a trainable weight matrix,  $(i)\boldsymbol{\alpha}$  and  $(i)\boldsymbol{\beta}$  are the adaptive soft weights for the event and frame branches, respectively. Here,  $(i)\sigma$  is a learned standard deviation that controls the magnitude of the noise perturbation, and  $\epsilon \sim \mathcal{N}(0, 1)$  represents a Gaussian noise term.

The fused feature map at each scale  $i$  is then obtained by applying the adaptive soft weights to the event and frame features:

$$(i)\mathbf{h}_{\text{fuse}}^a = (i)\boldsymbol{\alpha} \odot (i)\mathbf{h}_{\mathbf{E}}^a + (i)\boldsymbol{\beta} \odot (i)\mathbf{h}_{\mathbf{F}}, \quad (6)$$

<sup>1</sup>For simplicity, we use  $\mathbf{E}^b$  to represent a sample from the set of high-frequency event data  $\{\mathbf{E}_i^b\}_{i=0}^{b/a}$ , rather than explicitly referencing each individual sample from the event set. The same applies to other frequencies.

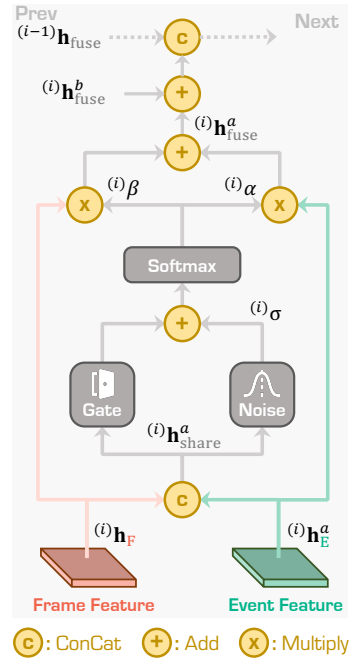


Figure 3: Illustration of the **FlexFuser** module. We show a general example of event and frame under frequency  $a$  at stage  $i$ .

where  $\odot$  denotes element-wise multiplication. This fusion process dynamically balances the contribution of each modality based on the input data, allowing for more robust and adaptive feature representation across varying conditions.

Then, at each scale  $i$ , the final feature map combining event data at different frequencies and the frame data is obtained by adding the fused features from the different frequencies. Specifically, we combine the fused feature maps as  $(^i)\mathbf{h}_{\text{fuse}} = (^i)\mathbf{h}_{\text{fuse}}^a + (^i)\mathbf{h}_{\text{fuse}}^b$ . After obtaining the fused feature maps across all scales, the multi-scale features are concatenated and fed into the detection head to produce the predicted bounding box  $\hat{\mathbf{y}}$ .

**Optimization & Regularization.** In addition to the standard detection loss  $\mathcal{L}_{\text{det}}(\mathbf{y}, \hat{\mathbf{y}})$ , we introduce a regularization term to ensure balanced utilization of both the event and RGB branches. This term penalizes large variations in the soft weights, encouraging a more uniform contribution from both modalities and preventing overfitting to a single branch:

$$\mathcal{L}_{\text{fuser}} = \mathcal{L}_{\text{det}}(\mathbf{y}, \hat{\mathbf{y}}) + \lambda \left( \frac{\text{Var}(\boldsymbol{\alpha})}{(\mathbb{E}[\boldsymbol{\alpha}])^2} + \frac{\text{Var}(\boldsymbol{\beta})}{(\mathbb{E}[\boldsymbol{\beta}])^2} \right), \quad (7)$$

where  $\lambda$  is a weighting factor.

### 3.3 FAL: FREQUENCY-ADAPTIVE LEARNING MECHANISM

FlexFuser aggregates information from different frequencies using labeled low-frequency data. To tune the model adaptively to handle diverse frequencies by leveraging both labeled low-frequency data and unlabeled high-frequency data, we design a flexible frequency-adaptive learning (**FAL**) mechanism. FAL incorporates multi-frequency information into the training process through iterative self-training. This approach enhances the model’s ability to generalize across varying frequencies, making it more robust in different scenarios. The key steps of the FAL mechanism are as follows:

**Pre-Training with Low-Frequency Labels.** Rather than training solely at the data collection frequency  $a$ , we enhance the model’s capability by training it at a higher frequency  $b$ . To efficiently leverage the available labels, we select only the final event from the high-frequency event set  $\{\mathbf{E}_i^b\}_{i=0}^{b/a}$ , which corresponds to the labeled timestamp. This approach allows the model to capture valuable high-frequency temporal information while still utilizing low-frequency labels, improving its temporal understanding and robustness. The training objective is to minimize the detection loss over the labeled data:

$$\mathcal{L}_{\text{GT}} = \sum_{(\mathbf{F}, \mathbf{E}_{b/a}^b, \mathbf{y}) \in \mathcal{D}} \mathcal{L}_{\text{det}}(\mathbf{y}, \hat{\mathbf{y}}). \quad (8)$$

**Labels at Higher Frequencies.** For the unlabeled data in  $\mathcal{D}$  captured at frequency  $b$ , the pre-trained model generates high-frequency labels  $\hat{\mathbf{y}}$  by performing inference on the entire high-frequency event set  $\{\mathbf{E}_i^b\}_{i=0}^{b/a}$ . These generated labels  $\hat{\mathbf{y}}$  serve as pseudo-labels for guiding further training at higher frequencies, improving the model’s ability to generalize across different temporal conditions.

**Enhanced Temporal Refinement.** To refine the high-frequency labels, we introduce a multi-step temporal refinement approach. First, we adopt bidirectional event augmentation by processing both forward and reversed event streams to detect objects with varying movements and orientations, thereby boosting recall. After generating the bidirectional labels, we apply Non-Maximum Suppression (NMS) to remove overlapping bounding boxes, followed by a low confidence threshold  $\tau$  to retain potential objects and further improve recall. Next, leveraging a tracking-by-detection framework, we link detection boxes across frames using pairwise IoU matching with a threshold  $\tau^{\text{IoU}}$ . Short-lived tracks, with lengths below  $\mathbf{L}^{\text{track}}$ , are pruned to ensure temporal consistency. This approach ensures that the refined high-frequency labels  $\tilde{\mathbf{y}}$  are accurate, temporally consistent, and reliable, ultimately improving detection quality in high-frequency data even in the absence of ground truth labels.

**Self-Training Iteration.** The model is iteratively trained using the refined high-frequency labels  $\tilde{\mathbf{y}}$  on high-frequency data where no ground truth labels are available. The total loss function combines the base training loss and the pseudo-label loss as:

$$\mathcal{L}_{\text{FAL}} = \mathcal{L}_{\text{GT}} + \beta \sum_{(\mathbf{F}, \{\mathbf{E}_i^b\}_{i=0}^{b/a-1}, \tilde{\mathbf{y}}) \in \mathcal{D}} \mathcal{L}_{\text{det}}(\tilde{\mathbf{y}}, \hat{\mathbf{y}}), \quad (9)$$

Table 1: Comparative study of state-of-the-art event camera detectors on the test set of *DSEC-Det* (Gehrig & Scaramuzza, 2024). Both event-only and event-frame fusion methods are compared. The **best** and 2nd best scores from each metric are highlighted in **bold** and underlined, respectively.

Modality	Method	Venue	Reference	mAP	$\text{AP}_{50}$	$\text{AP}_{75}$	$\text{AP}_{\text{S}}$	$\text{AP}_{\text{M}}$	$\text{AP}_{\text{L}}$
E	RVT	CVPR'23	(Gehrig & Scaramuzza, 2023)	38.4%	58.7%	41.3%	29.5%	50.3%	81.7%
	SAST	CVPR'24	(Peng et al., 2024)	38.1%	60.1%	40.0%	29.8%	48.9%	79.7%
	SSM	CVPR'24	(Zubić et al., 2024)	38.0%	55.2%	40.6%	28.8%	52.2%	77.8%
	LEOD	CVPR'24	(Wu et al., 2024)	41.1%	65.2%	43.6%	35.1%	47.3%	73.3%
E + F	DAGr-18	Nature'24	(Gehrig & Scaramuzza, 2024)	37.6%	-	-	-	-	-
	DAGr-34	Nature'24	(Gehrig & Scaramuzza, 2024)	39.0%	-	-	-	-	-
	DAGr-50	Nature'24	(Gehrig & Scaramuzza, 2024)	41.9%	66.0%	44.3%	36.3%	56.2%	77.8%
	<b>FlexEvent</b>	<b>Ours</b>	-	<b>57.4%</b>	<b>78.2%</b>	<b>66.6%</b>	<b>51.7%</b>	<b>64.9%</b>	<b>83.7%</b>

where  $\beta$  balances the contribution of the high-frequency label loss. The complete **FlexEvent** framework combines FlexFuser and FAL, allowing the model to dynamically fuse event and frame data while adapting to varying frequencies. As demonstrated in the following sections, this combination provides a robust detection framework capable of maintaining high accuracy in dynamic environments.

## 4 EXPERIMENTS

### 4.1 EXPERIMENTAL SETTINGS

**Datasets.** We conduct experiments based on three large-scale event camera datasets: <sup>1</sup>*DSEC-Det* (Gehrig & Scaramuzza, 2024), <sup>2</sup>*DSEC-Detection* (Tomy et al., 2022), and <sup>3</sup>*DSEC-MOD* (Zhou et al., 2023). These datasets comprise 78,344 frames across 60 sequences, 52,727 frames over 41 sequences, and 13,314 frames within 16 sequences, respectively, making them suitable for evaluating event-based object detection methods. We prioritize DSEC-Det as the primary benchmark for reporting results as it is the largest, most recent, and most comprehensive event-frame perception dataset. For more details, please refer to the Appendix.

**Baselines.** To evaluate our method, we compare it against both *event-only* and *event-frame fusion* state-of-the-art methods. For *event-only* detectors, we include RVT (Gehrig & Scaramuzza, 2023), SAST (Peng et al., 2024), LEOD (Wu et al., 2024), and SSM (Zubić et al., 2024), retraining them on the DSEC-Det dataset following their respective protocols. For *event-frame fusion* methods, we compare with DAGr (Gehrig & Scaramuzza, 2024) on DSEC-Det using results from the original paper and retrain our method on DSEC-Detection and DSEC-MOD using standard settings to compare with CAFR (Cao et al., 2024) and RENet (Zhou et al., 2023). For other methods on DSEC-Detection and DSEC-MOD, we reference results reported in the CAFR and RENet papers. For more details, please refer to the Appendix.

**Implementation Details.** We train our model using the YOLOX framework (Zheng et al., 2021), optimizing with the standard detection loss, which consists of IoU loss, classification loss, and regression loss, averaged across both the batch and sequence length for stable training. Additionally, we introduce an extra regularization term to balance the utilization among the different modalities. The model is trained for 100,000 iterations with a batch size of 8 and a sequence length of 11, using a learning rate of  $1 \times 10^{-4}$ . All experiments are conducted on two NVIDIA RTX A5000 GPUs with 24GB memory, with the entire training process completed in approximately one day. Due to space limits, more details are placed in the Appendix.

**Evaluation Metrics.** We evaluate object detectors using the mean Average Precision (mAP) as the primary metric, along with  $\text{AP}_{50}$ ,  $\text{AP}_{75}$ ,  $\text{AP}_{\text{S}}$ ,  $\text{AP}_{\text{M}}$ , and  $\text{AP}_{\text{L}}$  from the COCO evaluation protocol (Lin et al., 2014). These metrics provide a comprehensive assessment of detection performance across different IoU thresholds and object sizes. Kindly refer to the Appendix for more details.

### 4.2 COMPARISONS TO STATE-OF-THE-ART DETECTORS

**Comparison to Event-Only Models.** We compare **FlexEvent** with state-of-the-art event-only detectors, including RVT (Gehrig & Scaramuzza, 2023), SSM (Zubić et al., 2024), SAST (Peng et al., 2024), and LEOD (Wu et al., 2024), as shown in Tab. 1. We significantly outperform these methods

Table 2: Comparative study of state-of-the-art event camera detectors on the test set of *DSEC-Detection* (Tomy et al., 2022). Both event-only and event-frame fusion methods are compared. The reported results are the mAP scores of <sup>1</sup>Car, <sup>2</sup>Pedestrian (Ped), and <sup>3</sup>Large-Vehicle (L-Veh) classes. The **best** and 2nd best scores from each metric are highlighted in **bold** and underlined, respectively.

Modality	Method	Venue	Reference	Type	Car	Ped	L-Veh	Average
E	CAFR	ECCV'24	(Cao et al., 2024)	Event	-	-	-	12.0%
	SENet	CVPR'18	(Hu et al., 2018)	Attention	38.4%	14.9%	26.0%	26.2%
	CBAM	ECCV'18	(Woo et al., 2018)		37.7%	13.5%	27.0%	26.1%
	ECA-Net	CVPR'20	(Wang et al., 2020)		36.7%	12.8%	27.5%	25.7%
	SAGate	ECCV'20	(Chen et al., 2020)	RGB + Depth	32.5%	10.4%	16.0%	19.6%
	DCF	CVPR'21	(Ji et al., 2021)		36.3%	12.7%	28.0%	25.7%
	SPNet	ICCV'21	(Zhou et al., 2021)		39.2%	17.8%	26.2%	27.7%
E + F	RAMNet	RA-L'21	(Gehrig et al., 2021a)	RGB + Event	24.4%	10.8%	17.6%	17.6%
	FAGC	Sensors'21	(Cao et al., 2021)		39.8%	14.4%	33.6%	29.3%
	FPN-Fusion	ICRA'22	(Tomy et al., 2022)		37.5%	10.9%	24.9%	24.4%
	EFNet	ECCV'22	(Sun et al., 2022a)		41.1%	15.8%	32.6%	30.0%
	DRFuser	EAAI'23	(Munir et al., 2023)		38.6%	15.1%	30.6%	28.1%
	CMX	TITS'23	(Zhang et al., 2023)		41.6%	16.4%	29.4%	29.1%
	RENNet	ICRA'23	(Zhou et al., 2023)		40.5%	17.2%	30.6%	29.4%
	CAFR	ECCV'24	(Cao et al., 2024)		49.9%	25.8%	38.2%	38.0%
	<b>FlexEvent</b>	<b>Ours</b>	-		<b>59.3%</b>	<b>37.4%</b>	<b>45.5%</b>	<b>47.4%</b>

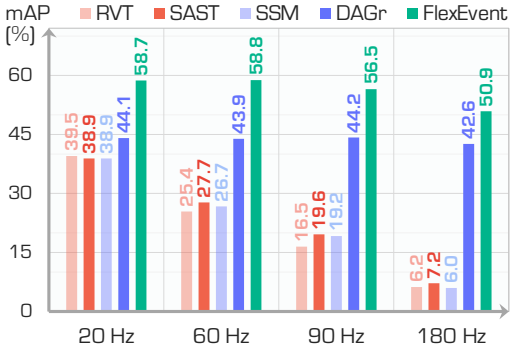


Figure 4: Comparisons of event-based detectors under different event frequencies on *DSEC-Det.*

across all metrics, with the performance gap becoming even more pronounced at higher frequencies. Event-only methods struggle to maintain detection accuracy at higher frequencies due to their inability to fully capture object semantics. In contrast, we overcome these limitations through the FlexFuser module, which integrates RGB data to compensate for the lack of semantic richness in the event stream. By fusing both event and frame data, we excel in complex and dynamic environments, achieving superior detection accuracy where event-only methods fall short.

**Comparison to Multimodal Models.** We compare **FlexEvent** with multimodal event-camera object detection methods such as DAGr (Gehrig & Scaramuzza, 2024), CAFR (Cao et al., 2024), and RENet (Zhou et al., 2023), which fuse event data with other sensor inputs, such as RGB frames or depth to improve detection accuracy. While these methods enhance performance over event-only approaches, they struggle to adapt to varying operational frequencies and often exhibit inadequate feature fusion in dynamic environments. Our approach addresses these limitations by dynamically balancing the contributions of event and frame data. As a result, we achieve superior performance, such as a 47.4% mAP on *DSEC-Detection* as shown in Tab. 2, outperforming CAFR (38.0%) and RENet (29.4%). This flexible combination of event and frame data, along with its ability to generalize across different temporal resolutions, enables our method to excel in high-frequency detection scenarios, surpassing state-of-the-art methods.

**Comparisons Across Different Categories.** We evaluate the performance of **FlexEvent** across various object categories, including cars, pedestrians, and large vehicles. As shown in Tab. 2, we consistently outperform other methods, achieving 59.3% mAP for cars, compared to 49.9% for CAFR (Cao et al., 2024). This highlights its effectiveness in detecting larger, fast-moving objects, while also surpassing CAFR in pedestrian categories. Existing methods struggle with detecting

Table 3: Comparisons of fusion-based event detectors on the test set of *DSEC-MOD* (Zhou et al., 2023). The **best** and 2nd best scores from each metric are highlighted in **bold** and underlined.

Method	Venue	Reference	mAP
SENet	CVPR'18	(Hu et al., 2018)	29.28%
CBAM	ECCV'18	(Woo et al., 2018)	36.22%
ECA-Net	CVPR'20	(Wang et al., 2020)	34.49%
SAGate	ECCV'20	(Chen et al., 2020)	33.62%
DCF	CVPR'21	(Ji et al., 2021)	32.20%
SPNet	ICCV'21	(Zhou et al., 2021)	32.70%
FPN-Fusion	ICRA'22	(Tomy et al., 2022)	32.28%
EFNet	ECCV'22	(Sun et al., 2022a)	35.33%
RENNet	ICRA'23	(Zhou et al., 2023)	38.38%
<b>FlexEvent</b>	<b>Ours</b>	-	<b>48.64%</b>

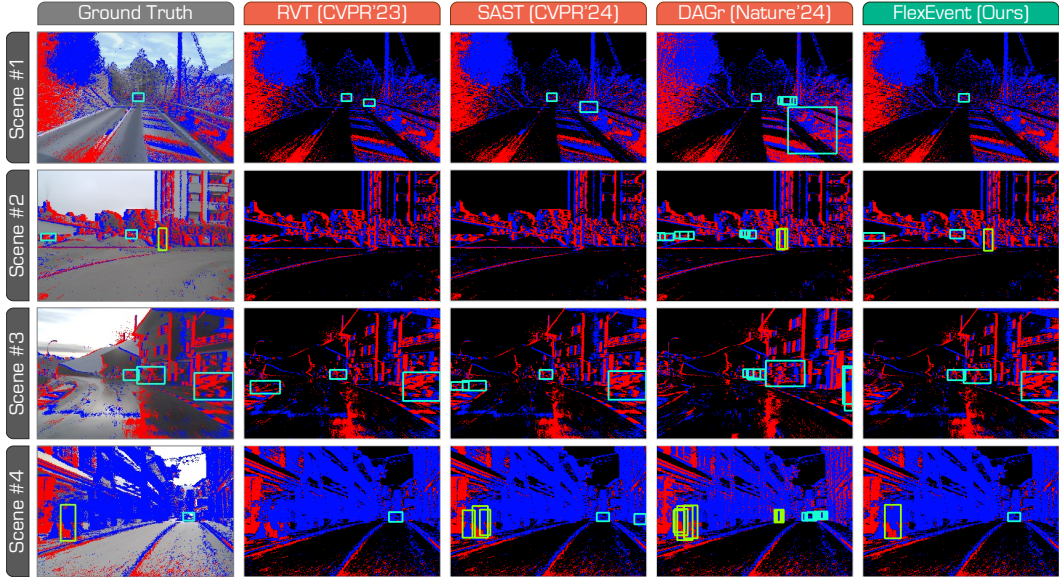


Figure 5: Qualitative results of state-of-the-art event camera detectors. We compare **FlexEvent** with RVT (Gehrig & Scaramuzza, 2023), SAST (Peng et al., 2024), and DAGr (Gehrig & Scaramuzza, 2024) on the test set of *DSEC-Det*. Best viewed in colors. See the Appendix for more examples.

Table 4: Ablation study of components in **FlexEvent**. **FlexFuser** denotes the adaptive event-frame fusion module (*cf.* Sec.3.2). **FAL** denotes the frequency-adaptive learning mechanism (*cf.* Sec. 3.3). The reported are the **mAP** scores on the test set of *DSEC-Det* (Gehrig & Scaramuzza, 2024). The symbol  $\diamond$  denotes the use of interpolated ground truth labels at high frequencies in **FAL**.

Modality	FAL	FlexFuser	Frequency (Hz)								Average
			20.0	27.5	30.0	36.0	45.0	60.0	90.0	180	
E	$\times$	$\times$	53.2%	54.0%	53.5%	52.0%	49.4%	45.9%	38.8%	22.9%	46.2%
	$\checkmark$	$\times$	54.6%	54.9%	54.9%	54.3%	53.3%	50.7%	44.6%	30.4%	49.7%
E + F	$\diamond$	$\checkmark$	54.9%	57.3%	57.7%	57.8%	57.2%	56.1%	53.7%	48.3%	55.4%
	$\times$	$\checkmark$	<b>58.0%</b>	59.6%	<b>60.0%</b>	59.6%	59.0%	57.6%	54.8%	49.2%	57.2%
	$\checkmark$	$\checkmark$	<b>57.4%</b>	<b>60.0%</b>	<b>60.0%</b>	<b>60.1%</b>	<b>59.5%</b>	<b>58.8%</b>	<b>56.5%</b>	<b>50.9%</b>	<b>57.9%</b>

smaller, slower-moving objects, especially in high-speed scenarios. Event-based detectors fail to detect stationary objects due to a lack of pixel intensity changes, and fusion methods over-rely on frame data, which lacks temporal resolution. Our approach addresses these issues with adaptive fusion and temporal refinement, ensuring accurate detection across different object types and motion dynamics. This versatility reinforces its superiority over state-of-the-art methods.

**Generalization on High-Frequency Data.** A key contribution of **FlexEvent** is its ability to generalize across various operational frequencies, particularly in high-frequency scenarios. We evaluate this by testing detection performance at different temporal offsets,  $\frac{i}{n} \Delta T$ , where  $n = 10$ ,  $i = 0, \dots, 10$ , and  $\Delta T = 50$  ms. Ground truth labels are generated by linearly interpolating object positions between frames for consistent evaluation. In this setting, event-based methods are tested across multiple time durations, while event-frame fusion methods process one RGB frame followed by event data of varying time durations. The comparison results are shown in Fig. 4. Most existing methods, such as RVT and SAST, struggle at higher frequencies due to their fixed temporal intervals and limited ability to capture fast scene changes. In contrast, our approach achieves 56.5% mAP at 90 Hz and 50.9% at 180 Hz. This improvement demonstrates that our method excels in dynamic, rapidly changing environments where accurate detection is critical for safety and reliability.

**Qualitative Assessment.** We provide qualitative comparisons between **FlexEvent** and other state-of-the-art methods under different event operation frequencies, as shown in Fig. 5 and Fig. 6. Unlike RVT and DAGr, which miss critical object details, our model consistently detects objects with high accuracy, even in challenging cases involving fast-moving vehicles and occluded pedestrians. For instance, in Scene 2 of Fig. 5, RVT fails to detect a pedestrian due to insufficient event data, while our approach successfully identifies the pedestrian by leveraging both frames and high-frequency event data. Similarly, in Scene 4, DAGr struggles with the rapid motion of a large vehicle, leading

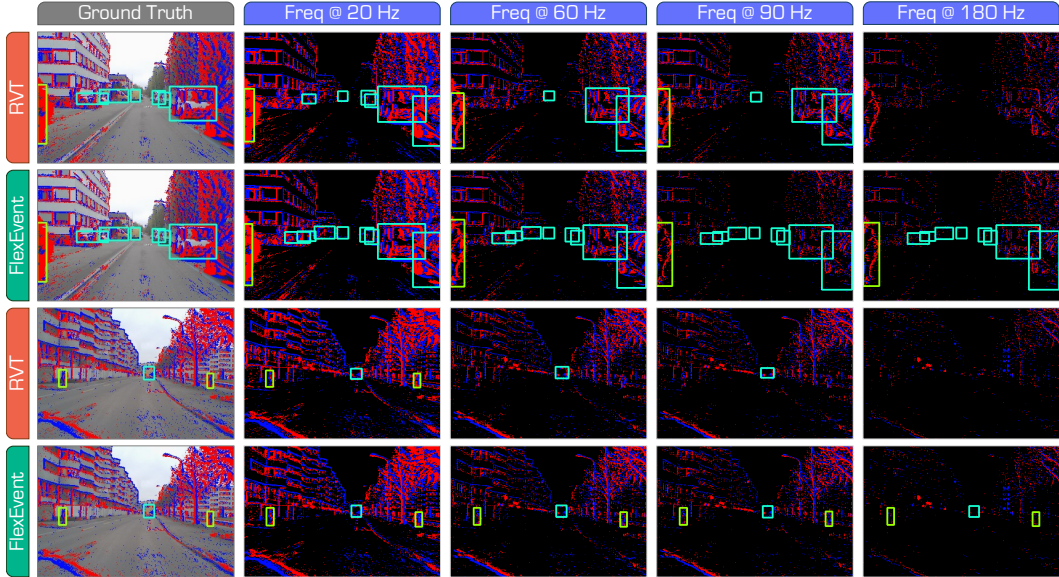


Figure 6: Qualitative comparisons of **FlexEvent** and **RVT** (Gehrig & Scaramuzza, 2023) under different event operation frequencies. Our approach demonstrates a strong robustness under both low- and high-frequency scenarios. Best viewed in colors. See the Appendix for more examples.

Table 5: Ablation study of hyperparameter configurations in the **FlexEvent** frameworks.  $\tau^{\text{car}}$ ,  $\tau^{\text{ped}}$  denotes the confidence threshold for car and pedestrian, respectively.  $\tau^{\text{iou}}$  denotes the IoU threshold when filter by tracking.  $L^{\text{track}}$  denotes the minimum track length. The reported results are the **mAP** scores on the test set of *DSEC-Det* (Gehrig & Scaramuzza, 2024).

$\tau^{\text{car}}$	$\tau^{\text{ped}}$	$L^{\text{track}}$	$\tau^{\text{iou}}$	Frequency (Hz)								<b>Average</b>
				20.0	27.5	30.0	36.0	45.0	60.0	90.0	180	
0.6	0.3	10	0.8	56.5%	55.9%	56.7%	57.2%	57.1%	56.7%	54.5%	49.2%	55.5%
0.6	0.3	10	0.6	56.7%	57.2%	57.7%	57.9%	57.7%	57.0%	54.3%	47.0%	55.7%
0.6	0.3	8	0.6	56.3%	58.5%	58.8%	59.1%	58.8%	58.4%	56.2%	51.2%	57.2%
0.6	0.3	6	0.6	57.3%	59.4%	59.7%	59.9%	59.3%	58.5%	55.7%	48.8%	57.3%
0.6	0.6	6	0.6	57.4%	60.0%	60.0%	60.1%	59.5%	58.8%	56.5%	50.9%	57.9%
0.8	0.8	6	0.6	56.6%	58.7%	59.1%	58.9%	58.4%	57.4%	55.6%	50.2%	56.9%

to inaccurate predictions, whereas our approach ensures precise object localization. In the upper instance of Fig. 6, RVT fails to detect a pedestrian at high frequency due to insufficient event data. In contrast, **FlexEvent** successfully identifies the pedestrian by leveraging the frame-based information. These qualitative findings confirm that our model excels not only in quantitative metrics but also in real-world performance.

#### 4.3 ABLATION STUDIES

**Component Analysis.** We conduct ablation studies by selectively removing key modules: the FlexFuser and FAL mechanisms. As shown in Tab. 4, removing the FAL mechanism results in a significant performance drop, particularly in high-frequency scenarios, underscoring its role in adapting to varying frequencies and generating frequency-adjusted labels. Similarly, omitting the FlexFuser module leads to a marked decrease in mAP, highlighting the importance of adaptive event-frame fusion for accurate detection across different operational frequencies. We also test training with interpolated labels for high-frequency testing, but this approach reduces recall by missing objects that suddenly appear or disappear, making it less effective than FAL.

**Hyperparameter Tuning.** We tune the hyperparameters of the FAL mechanism, focusing on key settings like the confidence threshold ( $\tau$ ), IoU threshold, and track length for temporal refinement. As shown in Tab. 5, lowering the confidence threshold improves recall but reduces precision, as the model becomes more lenient in detecting objects. Applying overly strict conditions, such as a higher confidence threshold or IoU threshold, lowers recall by filtering out valid detections. The optimal configuration is achieved with  $\tau = 0.6$  and a track length of 6, balancing precision and recall for both low- and high-frequency conditions. These moderate settings ensure that **FlexEvent** maintains robust performance and stable detection accuracy across diverse environments.

## 5 CONCLUSION

This paper introduces **FlexEvent**, an event-camera object detection framework designed to operate across arbitrary frequencies. By combining FlexFuser for adaptive event-frame fusion and FAL for frequency-adaptive learning, we leverage the rich temporal information of event data and the semantic detail of RGB frames to overcome the limitations of existing methods, providing a flexible solution for dynamic environments. Extensive experiments on large-scale datasets show that our approach significantly outperforms state-of-the-art methods, particularly in high-frequency scenarios, demonstrating its robustness and adaptability for real-world applications such as autonomous driving and robotics.

## APPENDIX

In this appendix, we supplement the following materials to support the findings and conclusions drawn in the main body of this paper.

<b>A Additional Implementation Details</b>	<b>11</b>
A.1 Datasets . . . . .	12
A.2 Baselines . . . . .	13
A.3 Evaluation Metrics . . . . .	13
A.4 Training & Inference Details . . . . .	14
<b>B Additional Quantitative Results</b>	<b>15</b>
B.1 Comparison of Efficiency . . . . .	15
B.2 Complete Results of Ablation Study . . . . .	15
B.3 Complete Results of Hyperparameter Searching . . . . .	15
<b>C Additional Qualitative Results</b>	<b>15</b>
C.1 Visual Comparisons of Event Camera Detectors . . . . .	15
C.2 Visual Comparisons under Different Frequencies . . . . .	15
<b>D Potential Societal Impact &amp; Limitations</b>	<b>15</b>
D.1 Societal Impact . . . . .	16
D.2 Broader Impact . . . . .	18
D.3 Known Limitations . . . . .	18
<b>E Public Resources Used</b>	<b>25</b>
E.1 Public Datasets Used . . . . .	25
E.2 Public Implementations Used . . . . .	25

## A ADDITIONAL IMPLEMENTATION DETAILS

In this section, to facilitate future reproductions, we elaborate on the necessary details in terms of the datasets, evaluation metrics, and implementation details adopted in our experiments.

Table 6: Summary of key statistics from the event camera object detection datasets used in this work.

Dataset	Reference	Classes	Frames	Sequences	Class Names
DSEC-MOD	(Zhou et al., 2023)	1	13, 314	16	Car
DSEC-Detection	(Tomy et al., 2022)	3	52, 727	41	Car Pedestrian Large-Vehicle
DSEC-Det	(Gehrig & Scaramuzza, 2024)	8	78, 344	60	Car Pedestrian Bus Bicycle Truck Motorcycle Rider Train

## A.1 DATASETS

In this work, we develop and validate our proposed approach on the large-scale DSEC dataset (Gehrig et al., 2021b). DSEC serves as a high-resolution, large-scale multimodal dataset designed to capture real-world driving scenarios under various conditions. It combines data from stereo Prophesee Gen3 event cameras with a resolution of  $640 \times 480$  pixels and FLIR Blackfly S RGB cameras operating at 20 FPS, enabling high-fidelity capture of dynamic scenes. To align the RGB frames with the event camera data, an infinite-depth alignment process is employed, which involves undistorting, rotating, and re-distorting the RGB images. This alignment ensures that the event data and RGB frames are temporally and spatially synchronized.

In our experiments, we utilize **three** comprehensive versions of DSEC tailored for object detection: *DSEC-Det* (Gehrig & Scaramuzza, 2024), *DSEC-Detection* (Tomy et al., 2022), and *DSEC-MOD* (Zhou et al., 2023). A summary of the key statistics of these datasets is listed in Tab. 6.

- **DSEC-Det** (Gehrig & Scaramuzza, 2024): This version is developed by the original DSEC team and includes annotations generated using the QDTrack multi-object tracker (Fischer et al., 2023; Pang et al., 2021). The annotation process combines automated multi-object tracking with manual refinement to ensure high-quality and accurate detection labels. Compared to the original DSEC dataset, DSEC-Det introduces additional sequences specifically designed to capture complex and dynamic urban environments, featuring crowded pedestrian areas, moving vehicles, and diverse lighting conditions. These challenging scenarios provide a rich testing ground for evaluating object detection algorithms in real-world driving settings. DSEC-Det comprises 60 sequences and 78, 344 frames, making it the most extensive dataset used in this study. It captures diverse urban scenes with dynamic elements, such as crowded pedestrian areas and moving vehicles. Covering eight object categories relevant to autonomous driving—Car, Pedestrian, Bus, Bicycle, Truck, Motorcycle, Rider, and Train—the dataset provides a robust foundation for training and evaluating object detection models across various driving scenarios. In our experiments on DSEC-Det, to maintain consistency with the experimental setup of previous work DAGr (Gehrig & Scaramuzza, 2024), we report results on two categories: Car and Pedestrian.
- **DSEC-Detection** (Tomy et al., 2022): This dataset comprises 41 sequences with a total of 52, 727 frames. Focusing on three fundamental object categories – Car, Pedestrian, and Large Vehicle – this version emphasizes high-precision annotations for these critical classes in autonomous driving. The initial annotations are generated using the YOLOv5 model (Jocher, 2020) on RGB frames, leveraging its robust performance in real-time object detection. These annotations are then transferred to the corresponding event frames through homographic transformation, ensuring spatial alignment between the two modalities. A subsequent manual refinement process corrects any discrepancies and enhances annotation quality, resulting in a dataset that provides accurate and reliable labels for event-based object detection.

- **DSEC-MOD** (Zhou et al., 2023): This dataset extends the object detection capabilities to moving-object detection across diverse urban environments. It includes 16 sequences containing 13,314 frames and is specifically focused on the Car category, making it highly suitable for complex detection tasks in varied urban settings, such as intersections, highways, and residential areas. Featuring high-frequency and dense annotations, the dataset provides a valuable resource for evaluating the performance of event-based object detectors under challenging real-world conditions.

These three versions of the DSEC dataset together provide a comprehensive platform for benchmarking and evaluating event-based object detection methods, capturing a wide spectrum of scenarios, object categories, and environmental conditions. Among them, DSEC-Det is the largest, most recent and most comprehensive, annotated and released by the original DSEC authors. Thus, we prioritize it as the primary benchmark for reporting results, ensuring relevance and reliability. DSEC-Detection and DSEC-MOD are datasets used by two recent event-frame fusion methods, CAFR (Cao et al., 2024) and RENet (Zhou et al., 2023). To validate the effectiveness of our method, we also report results on these two datasets.

## A.2 BASELINES

To evaluate the effectiveness of our method, we compare it against both event-only and event-frame fusion state-of-the-art methods.

- **Event-Only Methods.** We include state-of-the-art event-only object detectors, namely RVT (Gehrig & Scaramuzza, 2023), SAST (Peng et al., 2024), LEOD (Wu et al., 2024), and SSM (Zubić et al., 2024), which are originally trained on event-only datasets like Gen1 (De Tournemire et al., 2020) and 1Mpx (Perot et al., 2020). To ensure a fair comparison, we retrain these methods on the DSEC-Det dataset following their respective training protocols.
- **Event-Frame Fusion Methods.** For event-frame fusion methods on DSEC-Det, we include DAGr, as it has been evaluated on this dataset. We report the scores of DAGr (Gehrig & Scaramuzza, 2024) from the original paper to ensure consistency and fairness. For the DSEC-Detection and DSEC-MOD datasets, we train our model following the standard training and evaluation settings, and compare it against state-of-the-art methods CAFR (Cao et al., 2024) and RENet (Zhou et al., 2023), as reported in their respective papers. For other methods evaluated on DSEC-Detection and DSEC-MOD, we reference the results reported in the CAFR and RENet papers, respectively. Since DAGr’s training code is not publicly available, we could not reproduce its results on DSEC-Detection and DSEC-MOD.

These comparisons ensure a fair and comprehensive evaluation while adhering to resource and code availability constraints.

## A.3 EVALUATION METRICS

In this work, we adopt the mean Average Precision (**mAP**) as the primary metric to evaluate the performance of our object detection models, consistent with standard practices in the field. The mAP metric provides a comprehensive measure of detection accuracy across multiple categories and intersection-over-union (IoU) thresholds.

Mathematically, the **Average Precision (AP)** for a single class is calculated as:

$$\text{AP} = \int_0^1 p(r) dr \quad (10)$$

where  $p(r)$  represents the precision at a given recall level  $r$ . The mean Average Precision (mAP) is then computed as the mean of the AP values across all object categories and a range of IoU thresholds (typically from 0.5 to 0.95 with a step size of 0.05). This provides an overall measure of model performance across different levels of localization precision.

In addition to mAP, we also report the following metrics from the COCO evaluation protocol (Lin et al., 2014):

- $\text{AP}_{50}$ : The average precision when evaluated at a fixed IoU threshold of 0.50, indicating how well the model performs with relatively lenient localization criteria.
- $\text{AP}_{75}$ : The average precision at a fixed IoU threshold of 0.75, representing performance under stricter localization requirements.
- $\text{AP}_S$ ,  $\text{AP}_M$ , and  $\text{AP}_L$ : These metrics represent the average precision for small ( $S$ ), medium ( $M$ ), and large ( $L$ ) objects, respectively. Object sizes are defined based on their pixel area, with  $\text{AP}_S$  typically representing objects with areas less than  $32 \times 32$  pixels,  $\text{AP}_M$  representing areas between  $32 \times 32$  and  $96 \times 96$  pixels, and  $\text{AP}_L$  for objects larger than  $96 \times 96$  pixels.

By reporting these metrics, we obtain a more nuanced understanding of the model’s detection capabilities across varying object sizes and localization precision levels, ensuring a comprehensive evaluation of detection performance.

#### A.4 TRAINING & INFERENCE DETAILS

We train our models using mixed precision to optimize both memory efficiency and training speed. The training process spans 100,000 iterations, utilizing the ADAM optimizer (Kingma, 2014) with a OneCycle learning rate schedule (Smith & Topin, 2019), which gradually decays from a peak learning rate to enhance convergence.

Consistent with (Gehrig & Scaramuzza, 2023), we employ a mixed batching strategy to balance computational efficiency and memory usage. Specifically:

- Standard Backpropagation Through Time (BPTT): Applied to half of the training samples, allowing for full sequence training.
- Truncated BPTT (TBPTT): Used for the other half, reducing memory usage by splitting sequences into smaller segments.

For data augmentation, we apply random horizontal flipping and zoom transformations (both zoom-in and zoom-out) to enhance the diversity of training samples.

Our training process utilize the YOLOX framework (Zheng et al., 2021), a versatile object detection framework known for its efficient and high-performing architecture. We employ a multi-component loss function to optimize our model effectively:

- Intersection over Union (IoU) Loss: This loss component measures the overlap between the predicted bounding boxes and the ground-truth boxes, ensuring that the predicted regions closely match the actual object locations.
- Classification Loss: This component evaluates the accuracy of class predictions for each detected object, ensuring that the model correctly identifies the category of each detected instance.
- Regression Loss: This loss assesses the precision of the predicted bounding box coordinates, helping the model refine the location and size of bounding boxes to align closely with the ground-truth annotations.

To ensure stable training, these loss components are averaged across both the batch and sequence length at each optimization step. This averaging process helps to reduce variance during training and facilitates smoother convergence of the model parameters.

**Training Configuration.** The training is conducted with a batch size of 8, which provides an optimal balance between efficient GPU utilization and memory requirements. Each training sample contains a sequence length of 11 frames, allowing the model to learn temporal dependencies effectively. The learning rate is set to  $1 \times 10^{-4}$ , following a OneCycle learning rate schedule that allows efficient exploration of the learning space and helps in achieving faster convergence.

**Hardware & Training Time.** All training experiments are carried out on two NVIDIA RTX A5000 GPUs, each with 24GB of memory, providing the computational resources necessary for handling the high-resolution event data and RGB frames. The complete training process, including

Table 7: Comparative efficiency analysis of state-of-the-art event camera detectors on the test set of *DSEC-Det* (Gehrig & Scaramuzza, 2024), comparing both event-only and event-frame fusion methods. This table reports **inference times** at various frequencies, measured in **milliseconds (ms)**.

Modality	Method	Param (M)	Frequency (Hz)								
			20.0	27.5	30	36	45	60	90	180	200
E	RVT	18.5	9.20	8.67	8.35	7.93	7.61	7.51	7.19	6.77	6.34
	SAST	18.9	14.06	13.11	12.68	12.37	11.95	11.63	11.52	11.10	10.36
	SSM	18.2	8.79	8.26	8.08	7.71	7.55	7.30	6.90	6.54	6.12
E + F	DAGr-50	34.6	73.35	65.73	60.02	55.11	51.00	48.00	45.29	43.89	37.58
	FlexEvent	45.4	14.27	13.53	13.32	13.00	12.79	12.58	12.47	12.37	12.12

all iterations and model optimization, takes approximately one day, demonstrating the efficiency of our implementation in terms of both training speed and resource utilization.

## B ADDITIONAL QUANTITATIVE RESULTS

### B.1 COMPARISON OF EFFICIENCY

We present a comparative analysis of inference times and parameter counts for the evaluated methods in Tab. 7. All experiments are conducted on an NVIDIA RTX A5000 24GB GPU paired with an AMD EPYC 9354P 32-Core Processor operating at 3.8 GHz. The results demonstrate that, despite having a higher parameter count, FlexEvent achieves inference times comparable to the event-only method SAST and significantly outperforms the event-frame fusion method DAGr in terms of speed. Additionally, FlexEvent consistently surpasses DAGr in inference time across all tested frequencies. These results underscore the efficiency and rapid performance of FlexEvent, highlighting its suitability for real-time applications.

### B.2 COMPLETE RESULTS OF ABLATION STUDY

We include the complete results of the ablation study in Tab. 8.

### B.3 COMPLETE RESULTS OF HYPERPARAMETER SEARCHING

We include the complete results of the hyperparameter searching in Tab. 9.

## C ADDITIONAL QUALITATIVE RESULTS

### C.1 VISUAL COMPARISONS OF EVENT CAMERA DETECTORS

We include additional qualitative assessments in Fig. 7, Fig. 8, and Fig. 9.

### C.2 VISUAL COMPARISONS UNDER DIFFERENT FREQUENCIES

We include additional qualitative assessments in Fig. 10, Fig. 11, and Fig. 12.

## D POTENTIAL SOCIETAL IMPACT & LIMITATIONS

In this section, we discuss the potential societal impact of FlexEvent, including its positive contributions, broader implications, and known limitations. While our method offers significant advancements in event camera object detection, it is important to consider its broader consequences and areas for future improvement.

Table 8: The complete results of the ablation study (*cf.* Tab. 4) of different components in the **FlexEvent** framework. **FlexFuser** denotes the adaptive event-frame fusion module (*cf.* Sec. 3.2). **FAL** denotes the frequency-adaptive learning module (*cf.* Sec. 3.3). The reported results are the **mAP**, **AP<sub>50</sub>**, **AP<sub>75</sub>**, **AP<sub>S</sub>**, **AP<sub>M</sub>**, and **AP<sub>L</sub>** scores on the test set of *DSEC-Det* (Gehrig & Scaramuzza, 2024). The symbol ♦ denotes the use of interpolated ground truth labels at high frequencies in **FAL**. The **best** and 2nd best scores of each metric are highlighted in **bold** and underline, respectively.

Modality	FAL	FlexFuser	Frequency (Hz)	mAP	AP <sub>50</sub>	AP <sub>75</sub>	AP <sub>S</sub>	AP <sub>M</sub>	AP <sub>L</sub>
Event	✗	✗	20.0	53.2%	<b>77.2%</b>	<u>58.1%</u>	<b>46.4%</b>	64.4%	83.0%
	✗	✗	27.5	<b>54.0%</b>	76.8%	<b>59.3%</b>	<b>46.4%</b>	66.6%	<b>85.2%</b>
	✗	✗	30.0	<u>53.5%</u>	75.5%	<b>59.3%</b>	<u>45.6%</u>	<b>66.8%</b>	85.0%
	✗	✗	36.0	52.0%	73.3%	<u>58.1%</u>	44.0%	65.5%	84.9%
	✗	✗	45.0	49.4%	69.5%	55.4%	40.7%	64.1%	84.3%
	✗	✗	60.0	45.9%	64.2%	51.8%	36.5%	62.3%	82.7%
	✗	✗	90.0	38.8%	55.4%	43.9%	28.5%	55.3%	79.9%
	✗	✗	180.0	22.9%	36.1%	23.9%	14.1%	34.5%	60.1%
Event	✓	✗	20.0	54.6%	<b>79.1%</b>	<b>61.8%</b>	<u>47.4%</u>	64.4%	81.4%
	✓	✗	27.5	<b>54.9%</b>	78.8%	<u>61.4%</u>	<b>47.6%</b>	66.1%	83.2%
	✓	✗	30.0	<b>54.9%</b>	78.5%	<u>61.3%</u>	<b>47.4%</b>	<b>66.9%</b>	83.3%
	✓	✗	36.0	54.3%	77.1%	60.5%	46.8%	<u>66.7%</u>	83.4%
	✓	✗	45.0	53.3%	75.3%	59.8%	45.6%	65.4%	<b>83.8%</b>
	✓	✗	60.0	50.7%	72.4%	57.3%	42.3%	63.5%	<u>83.5%</u>
	✓	✗	90.0	44.6%	65.1%	49.9%	35.3%	58.9%	81.9%
	✓	✗	180.0	30.4%	48.1%	32.2%	20.7%	44.0%	72.9%
Event + Frame	♦	✓	20.0	54.9%	74.0%	63.2%	50.7%	61.3%	85.5%
	♦	✓	27.5	57.3%	75.7%	66.3%	<b>52.8%</b>	65.8%	86.9%
	♦	✓	30.0	<u>57.7%</u>	<b>75.9%</b>	<b>66.8%</b>	<u>52.7%</u>	67.2%	<b>87.5%</b>
	♦	✓	36.0	<b>57.8%</b>	75.7%	<u>66.5%</u>	52.5%	67.9%	<u>87.2%</u>
	♦	✓	45.0	57.2%	75.5%	65.4%	51.6%	<b>68.2%</b>	<b>87.5%</b>
	♦	✓	60.0	56.1%	74.2%	63.4%	50.1%	68.1%	86.5%
	♦	✓	90.0	53.7%	72.2%	59.5%	47.1%	66.2%	85.7%
	♦	✓	180.0	48.3%	66.9%	52.2%	40.8%	60.6%	84.2%
Event + Frame	✗	✓	20.0	58.0%	76.5%	66.4%	52.7%	66.2%	86.3%
	✗	✓	27.5	<b>59.6%</b>	<b>78.2%</b>	<b>69.6%</b>	<b>54.1%</b>	69.9%	<b>88.0%</b>
	✗	✓	30.0	<b>60.0%</b>	78.1%	69.5%	<u>53.7%</u>	<b>71.3%</b>	<u>87.8%</u>
	✗	✓	36.0	<u>59.6%</u>	77.2%	68.6%	53.1%	71.1%	87.7%
	✗	✓	45.0	59.0%	76.7%	67.1%	52.1%	<u>71.1%</u>	<u>87.8%</u>
	✗	✓	60.0	57.6%	75.2%	65.6%	50.2%	70.6%	87.2%
	✗	✓	90.0	54.8%	72.6%	61.9%	46.8%	68.8%	86.3%
	✗	✓	180.0	49.2%	67.4%	53.5%	40.8%	62.3%	85.4%
Event + Frame	✓	✓	20.0	57.4%	78.2%	66.6%	51.7%	64.9%	83.7%
	✓	✓	27.5	60.0%	79.4%	<u>70.1%</u>	<u>53.5%</u>	68.4%	<b>86.1%</b>
	✓	✓	30.0	<u>60.0%</u>	<b>79.7%</b>	<b>70.8%</b>	<b>53.6%</b>	69.9%	<b>86.1%</b>
	✓	✓	36.0	<b>60.1%</b>	79.6%	<b>70.8%</b>	53.2%	70.3%	<u>85.7%</u>
	✓	✓	45.0	59.5%	79.0%	69.5%	52.5%	<u>70.8%</u>	85.3%
	✓	✓	60.0	58.8%	78.5%	69.0%	51.1%	<b>71.1%</b>	85.3%
	✓	✓	90.0	56.5%	76.5%	65.4%	48.2%	70.1%	83.8%
	✓	✓	180.0	50.9%	71.4%	56.2%	41.6%	65.4%	82.9%

## D.1 SOCIETAL IMPACT

The development of **FlexEvent** introduces several positive societal benefits, particularly in safety-critical applications such as autonomous driving, robotics, and surveillance. By enhancing the ability to detect fast-moving objects in real time, our framework can improve the responsiveness and safety of autonomous systems operating in dynamic environments. This is especially important for avoiding collisions or responding to hazards in high-speed scenarios. For example, autonomous vehicles equipped with our approach can better detect pedestrians, cyclists, and other vehicles in real time, potentially reducing accidents and saving lives.

Additionally, the computational efficiency provided by the adaptive event-frame fusion (FlexFuser) and frequency-adaptive learning (FAL) mechanisms reduces the need for resource-intensive training processes. This contributes to the broader societal goal of making advanced AI technologies more accessible and less energy-intensive, thereby minimizing the environmental impact of large-scale

Table 9: The complete results of the ablation study (*cf.* Tab. 5) of different hyperparameter configurations in the **FlexEvent** framework.  $\tau^{\text{car}}$ ,  $\tau^{\text{ped}}$  denotes the confidence threshold for car and pedestrian, respectively.  $\tau^{\text{iou}}$  denotes the IoU threshold when filter by tracking,  $L^{\text{track}}$  denotes the minimum track length. The reported results are the **mAP** scores on the test set of *DSEC-Det* (Gehrig & Scaramuzza, 2024). The **best** and 2nd best scores of each metric from each hyperparameter configuration are highlighted in **bold** and underline, respectively.

$\tau^{\text{car}}$	$\tau^{\text{ped}}$	$L^{\text{track}}$	$\tau^{\text{iou}}$	Frequency (Hz)	mAP	$\text{AP}_{\text{50}}$	$\text{AP}_{\text{75}}$	$\text{AP}_{\text{S}}$	$\text{AP}_{\text{M}}$	$\text{AP}_{\text{L}}$
0.6	0.3	10	0.8	20.0	56.5%	<b>81.3%</b>	66.4%	51.8%	62.2%	82.8%
0.6	0.3	10	0.8	27.5	55.9%	74.7%	65.1%	51.9%	61.4%	87.0%
0.6	0.3	10	0.8	30.0	56.7%	75.3%	66.0%	<u>52.3%</u>	63.5%	87.0%
0.6	0.3	10	0.8	36.0	<b>57.2%</b>	<b>75.9%</b>	<b>67.0%</b>	<b>52.5%</b>	64.8%	86.9%
0.6	0.3	10	0.8	45.0	57.1%	75.7%	66.2%	51.5%	66.1%	<u>87.2%</u>
0.6	0.3	10	0.8	60.0	56.7%	75.3%	65.7%	50.3%	<b>67.4%</b>	<b>87.3%</b>
0.6	0.3	10	0.8	90.0	54.5%	73.2%	62.3%	47.3%	<u>66.3%</u>	86.2%
0.6	0.3	10	0.8	180.0	49.2%	68.2%	54.2%	40.8%	62.4%	85.5%
0.6	0.3	10	0.6	20.0	56.7%	<b>80.6%</b>	65.5%	51.2%	63.0%	81.7%
0.6	0.3	10	0.6	27.5	57.2%	79.3%	65.0%	51.9%	65.2%	84.5%
0.6	0.3	10	0.6	30.0	57.7%	79.4%	66.0%	<b>52.3%</b>	66.3%	85.0%
0.6	0.3	10	0.6	36.0	<b>57.9%</b>	79.5%	<b>66.4%</b>	52.2%	66.8%	84.8%
0.6	0.3	10	0.6	45.0	57.7%	79.2%	65.6%	<u>51.7%</u>	<b>67.1%</b>	85.1%
0.6	0.3	10	0.6	60.0	57.0%	78.8%	64.8%	50.5%	<b>67.6%</b>	<b>85.3%</b>
0.6	0.3	10	0.6	90.0	54.3%	76.4%	60.0%	46.9%	66.3%	84.5%
0.6	0.3	10	0.6	180.0	47.0%	69.0%	49.1%	37.8%	61.1%	83.9%
0.6	0.3	8	0.6	20.0	56.3%	77.2%	64.9%	50.4%	64.1%	83.3%
0.6	0.3	8	0.6	27.5	58.5%	78.3%	68.1%	52.5%	66.8%	84.8%
0.6	0.3	8	0.6	30.0	58.8%	78.5%	68.7%	52.6%	67.9%	85.7%
0.6	0.3	8	0.6	36.0	<b>59.1%</b>	<b>78.8%</b>	<b>69.0%</b>	<b>52.7%</b>	<u>68.8%</u>	<b>86.5%</b>
0.6	0.3	8	0.6	45.0	58.8%	78.2%	68.6%	52.3%	<u>68.8%</u>	86.1%
0.6	0.3	8	0.6	60.0	58.4%	77.9%	67.5%	51.3%	<b>69.6%</b>	85.5%
0.6	0.3	8	0.6	90.0	56.2%	76.6%	64.8%	48.5%	68.3%	84.7%
0.6	0.3	8	0.6	180.0	51.2%	71.9%	56.3%	42.6%	64.2%	82.9%
0.6	0.3	6	0.6	20.0	57.3%	80.0%	65.2%	51.2%	65.8%	84.1%
0.6	0.3	6	0.6	27.5	59.4%	81.3%	<u>68.5%</u>	53.4%	68.8%	<b>85.7%</b>
0.6	0.3	6	0.6	30.0	59.7%	<b>81.7%</b>	<b>69.0%</b>	<b>53.7%</b>	69.0%	85.3%
0.6	0.3	6	0.6	36.0	<b>59.9%</b>	81.4%	<b>69.0%</b>	53.6%	<b>69.8%</b>	<b>85.7%</b>
0.6	0.3	6	0.6	45.0	59.3%	80.5%	67.9%	52.8%	69.4%	85.6%
0.6	0.3	6	0.6	60.0	58.5%	79.6%	67.0%	51.5%	<u>69.6%</u>	84.9%
0.6	0.3	6	0.6	90.0	55.7%	77.2%	62.8%	48.1%	67.9%	84.3%
0.6	0.3	6	0.6	180.0	48.8%	70.6%	50.9%	40.8%	61.1%	83.4%
0.6	0.6	6	0.6	20.0	57.4%	78.2%	66.6%	51.7%	64.9%	83.7%
0.6	0.6	6	0.6	27.5	60.0%	79.4%	<u>70.1%</u>	53.5%	68.4%	<b>86.1%</b>
0.6	0.6	6	0.6	30.0	60.0%	<b>79.7%</b>	<b>70.8%</b>	<b>53.6%</b>	69.9%	<b>86.1%</b>
0.6	0.6	6	0.6	36.0	<b>60.1%</b>	79.6%	<b>70.8%</b>	53.2%	70.3%	<u>85.7%</u>
0.6	0.6	6	0.6	45.0	59.5%	79.0%	69.5%	52.5%	<u>70.8%</u>	85.3%
0.6	0.6	6	0.6	60.0	58.8%	78.5%	69.0%	51.1%	<b>71.1%</b>	85.3%
0.6	0.6	6	0.6	90.0	56.5%	76.5%	65.4%	48.2%	70.1%	83.8%
0.6	0.6	6	0.6	180.0	50.9%	71.4%	56.2%	41.6%	65.4%	82.9%
0.8	0.8	6	0.6	20.0	56.6%	80.7%	65.5%	50.8%	65.4%	82.6%
0.8	0.8	6	0.6	27.5	58.7%	81.9%	<u>68.9%</u>	<b>52.8%</b>	68.6%	84.9%
0.8	0.8	6	0.6	30.0	<b>59.1%</b>	<b>82.0%</b>	<b>69.2%</b>	<u>52.7%</u>	69.5%	84.8%
0.8	0.8	6	0.6	36.0	58.9%	81.7%	68.8%	52.6%	<b>69.9%</b>	85.0%
0.8	0.8	6	0.6	45.0	58.4%	81.4%	67.7%	51.6%	69.8%	<b>85.1%</b>
0.8	0.8	6	0.6	60.0	57.4%	80.1%	66.6%	50.2%	<b>69.9%</b>	84.3%
0.8	0.8	6	0.6	90.0	55.7%	78.6%	63.7%	47.8%	68.9%	84.2%
0.8	0.8	6	0.6	180.0	50.2%	74.0%	55.2%	41.5%	63.7%	83.1%

AI models. Our approach could also benefit industries beyond transportation, such as robotics for healthcare, industrial automation, and public safety.

## D.2 BROADER IMPACT

The broader implications of **FlexEvent** include its potential to advance the field of event-based vision and enable new applications where high temporal resolution is crucial. By overcoming the limitations of conventional fixed-frequency object detection methods, our approach paves the way for more flexible, adaptable AI systems. This could lead to improvements in areas such as drone navigation, real-time video analysis for security purposes, and human-robot collaboration, where detecting fast-moving objects and adapting to changing environments are critical.

Moreover, the development of efficient and scalable detection systems like our approach can drive further innovation in resource-constrained environments, such as low-power edge devices. These advancements could make high-performance detection systems more widely available, particularly in developing regions or areas with limited access to computational resources.

However, as with any powerful technology, there is a risk of misuse. Enhanced object detection capabilities could potentially be exploited for surveillance purposes, raising privacy concerns. As event camera technology becomes more widespread, it is important to establish ethical guidelines and regulatory frameworks to ensure that these systems are used responsibly, particularly when monitoring public spaces or collecting sensitive data.

## D.3 KNOWN LIMITATIONS

While **FlexEvent** demonstrates significant performance improvements, there are several known limitations to our approach.

**Dependence on Event Camera Quality.** The effectiveness of our approach relies on the quality of the event camera sensor. Inconsistent or noisy event data, especially under poor lighting or extreme weather conditions, could affect detection performance. Future work could explore robustness to sensor noise and adaptation to diverse environmental conditions.

**Limited Generalization to Unseen Scenarios.** Although our approach shows strong performance across varying frequencies, it may still face challenges in completely unseen environments, where the motion dynamics and scene conditions differ significantly from the training data. Investigating methods for domain adaptation or online learning could help improve generalization to new contexts.

**Resource Requirements for High-Frequency Data.** While FlexFuser mitigates the computational cost of training on high-frequency event data, processing extremely high-frequency event streams still requires substantial computational resources during inference. This could limit the scalability on resource-constrained devices or in real-time applications with stringent latency requirements.

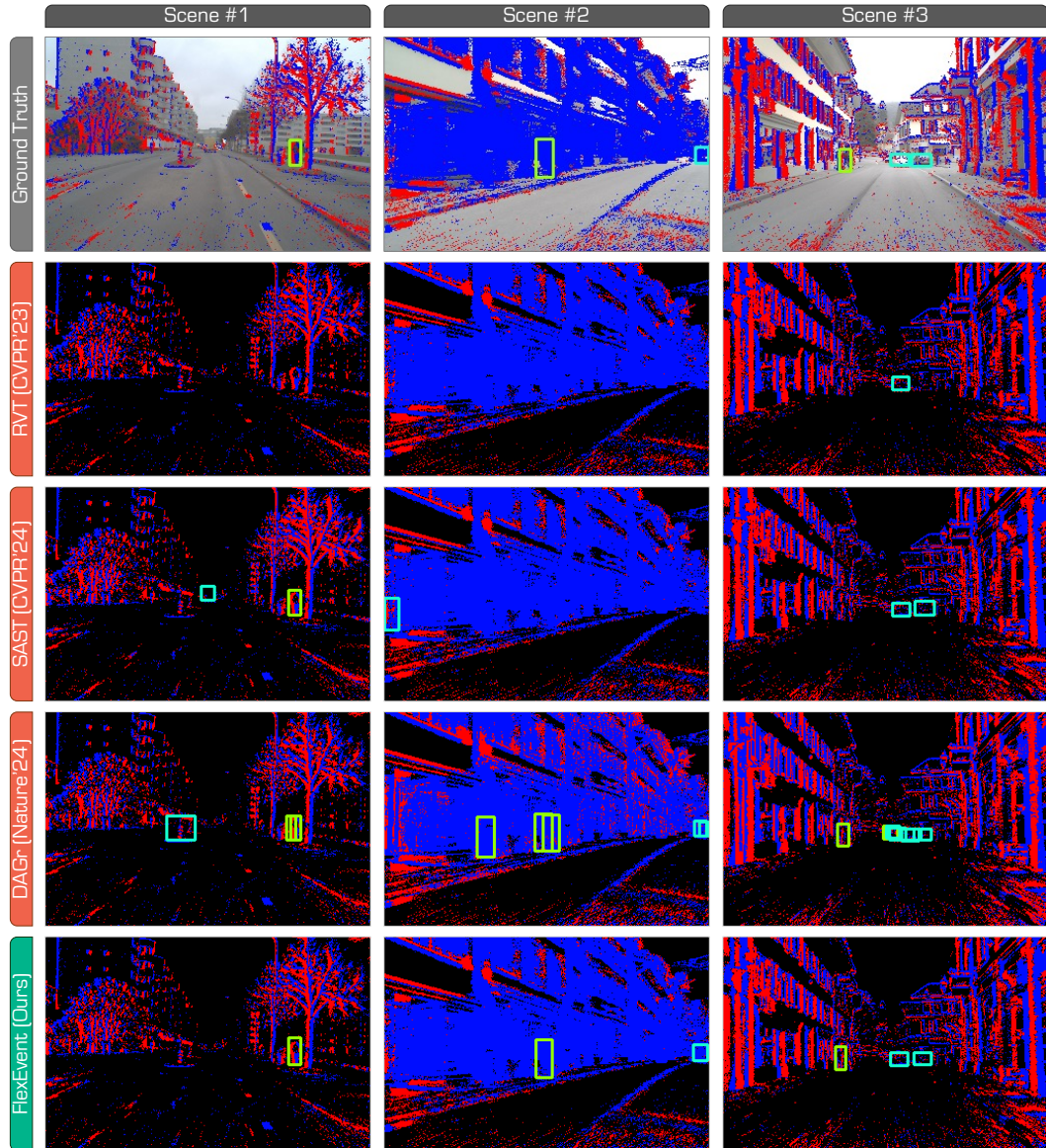


Figure 7: Additional qualitative results of state-of-the-art event camera detectors. We compare the proposed **FlexEvent** with RVT (Gehrig & Scaramuzza, 2023), SAST (Peng et al., 2024), and DAGr (Gehrig & Scaramuzza, 2024) on the test set of *DSEC-Det*. Best viewed in colors.

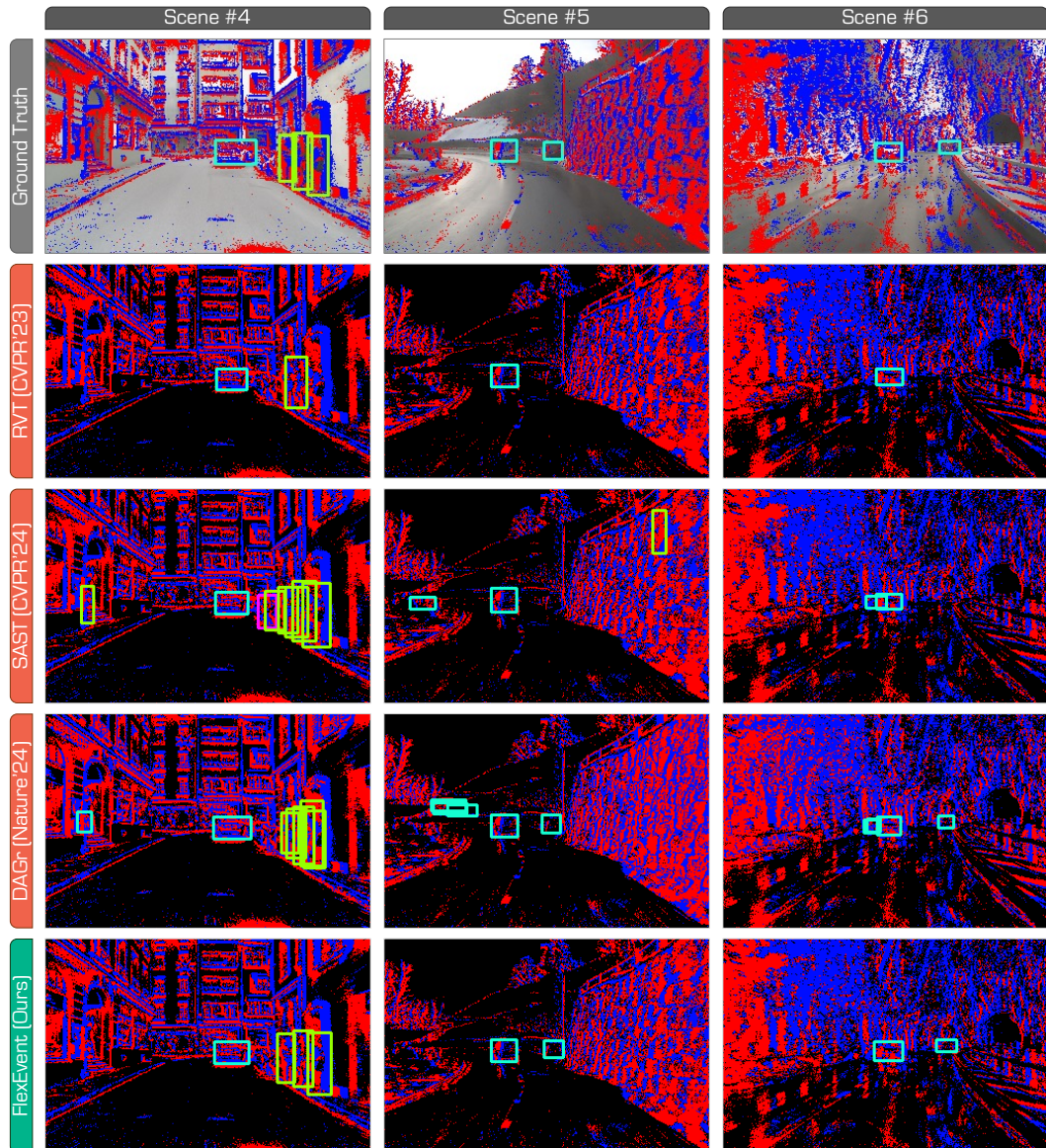


Figure 8: Additional qualitative results of state-of-the-art event camera detectors. We compare the proposed **FlexEvent** with RVT (Gehrig & Scaramuzza, 2023), SAST (Peng et al., 2024), and DAGr (Gehrig & Scaramuzza, 2024) on the test set of *DSEC-Det*. Best viewed in colors.

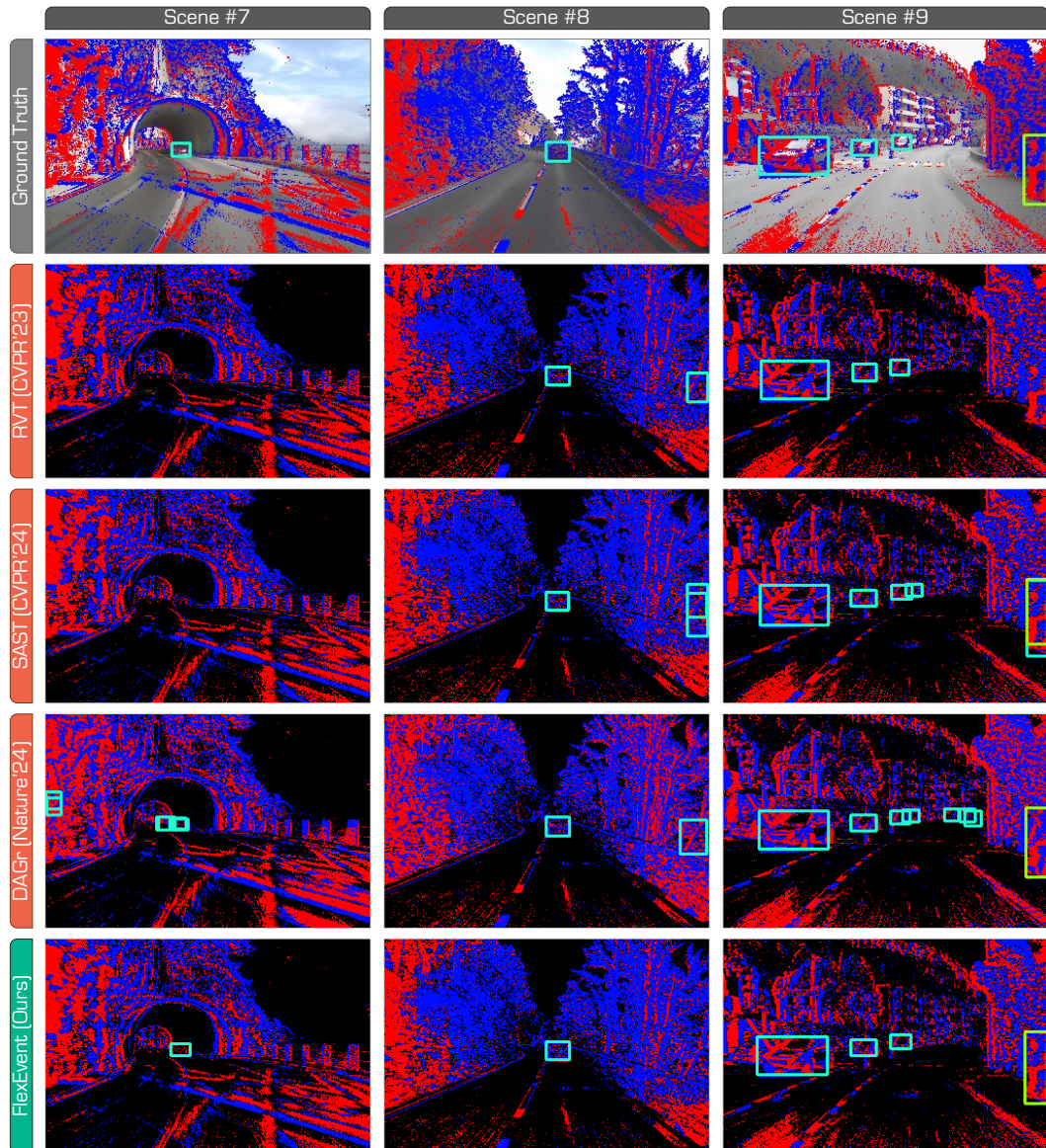


Figure 9: Additional qualitative results of state-of-the-art event camera detectors. We compare the proposed **FlexEvent** with RVT (Gehrig & Scaramuzza, 2023), SAST (Peng et al., 2024), and DAGr (Gehrig & Scaramuzza, 2024) on the test set of *DSEC-Det*. Best viewed in colors.

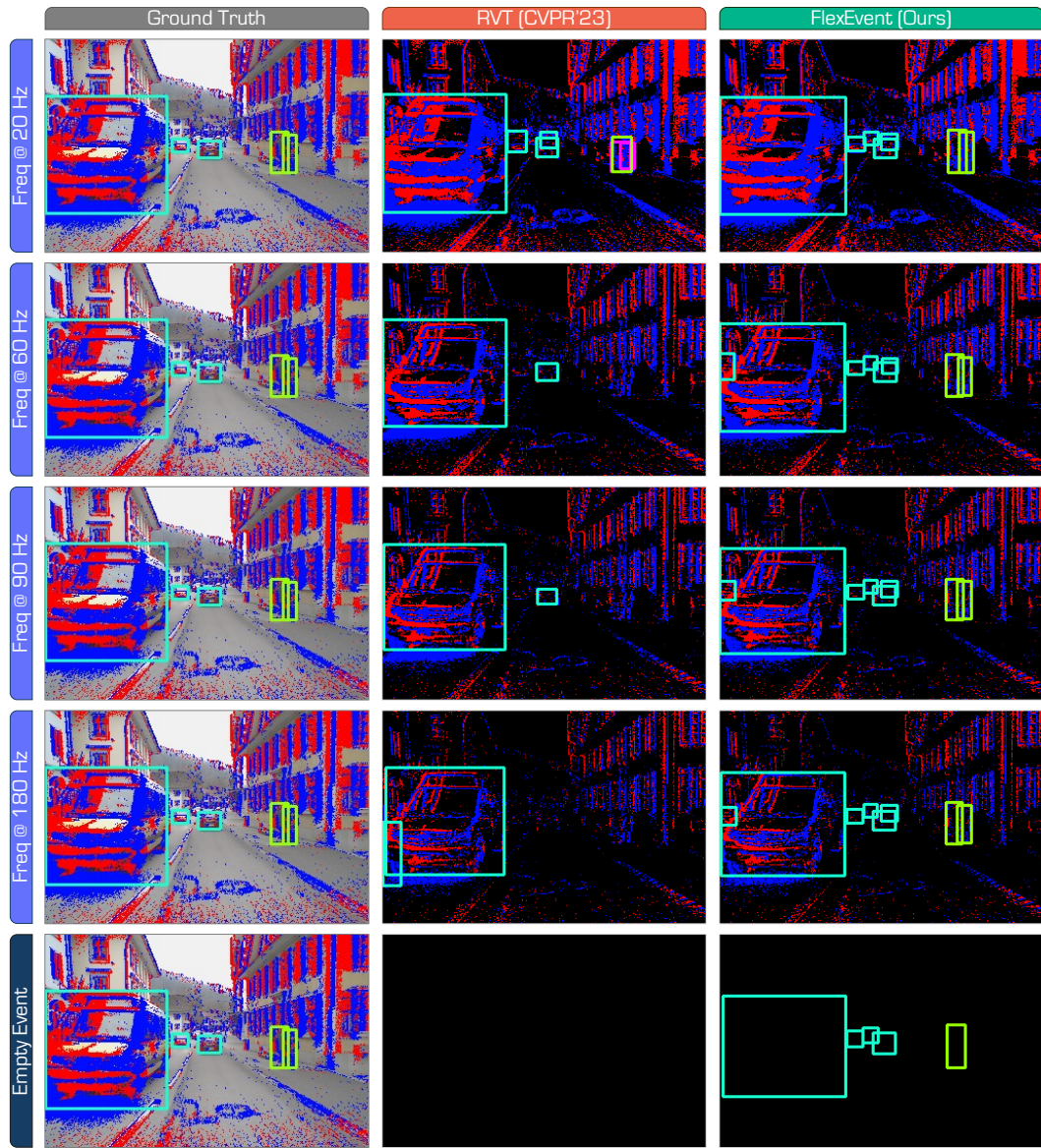


Figure 10: Additional qualitative comparisons of the RVT model (Gehrig & Scaramuzza, 2023) and the proposed **FlexEvent** under different event camera operation frequencies (20 Hz, 60 Hz, 90 Hz, and 180 Hz) and the empty event scenario. The experiments are conducted on the test set of *DSEC-Det*. Best viewed in colors.

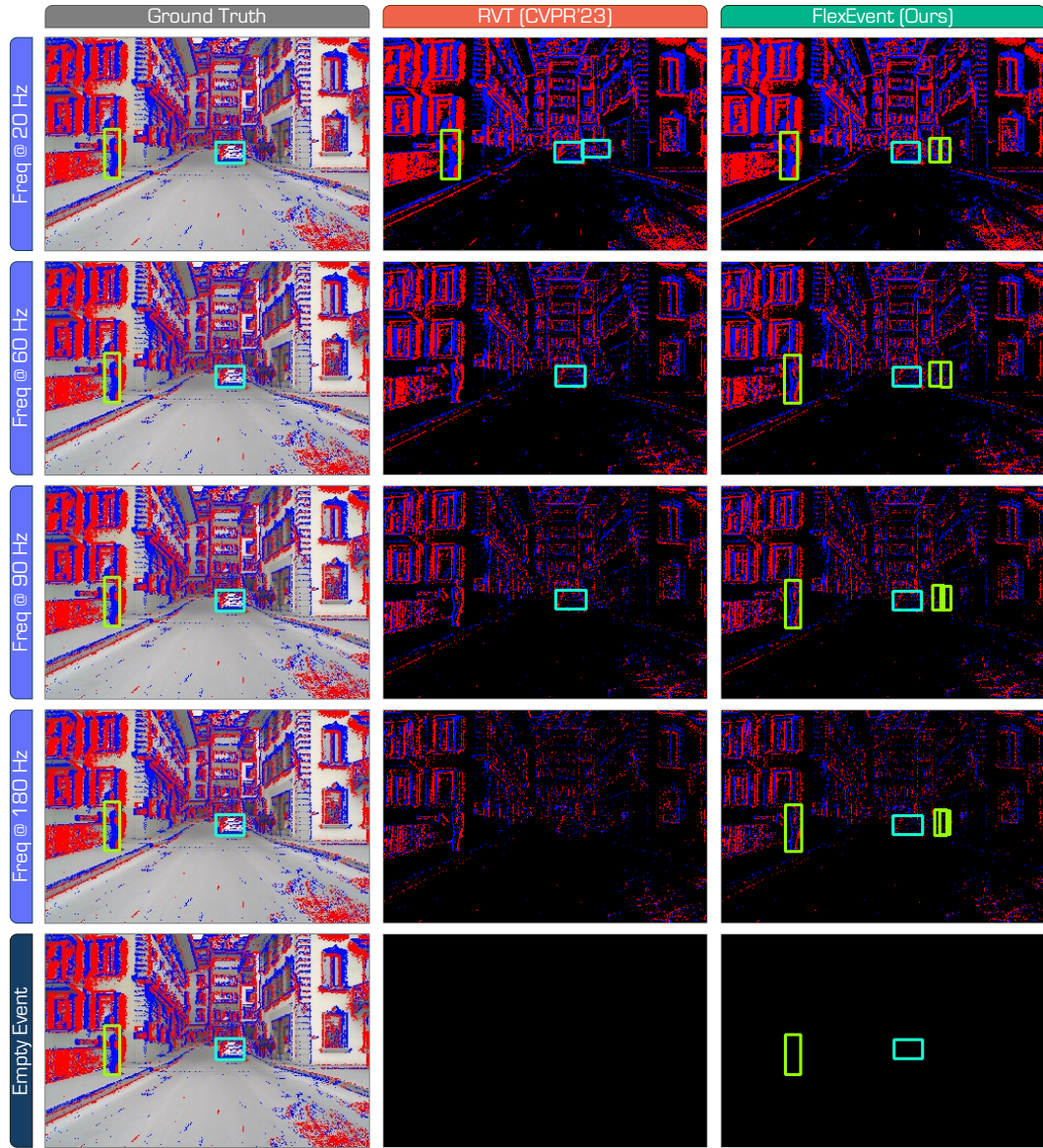


Figure 11: Additional qualitative comparisons of the RVT model (Gehrig & Scaramuzza, 2023) and the proposed **FlexEvent** under different event camera operation frequencies (20 Hz, 60 Hz, 90 Hz, and 180 Hz) and the empty event scenario. The experiments are conducted on the test set of *DSEC-Det*. Best viewed in colors.

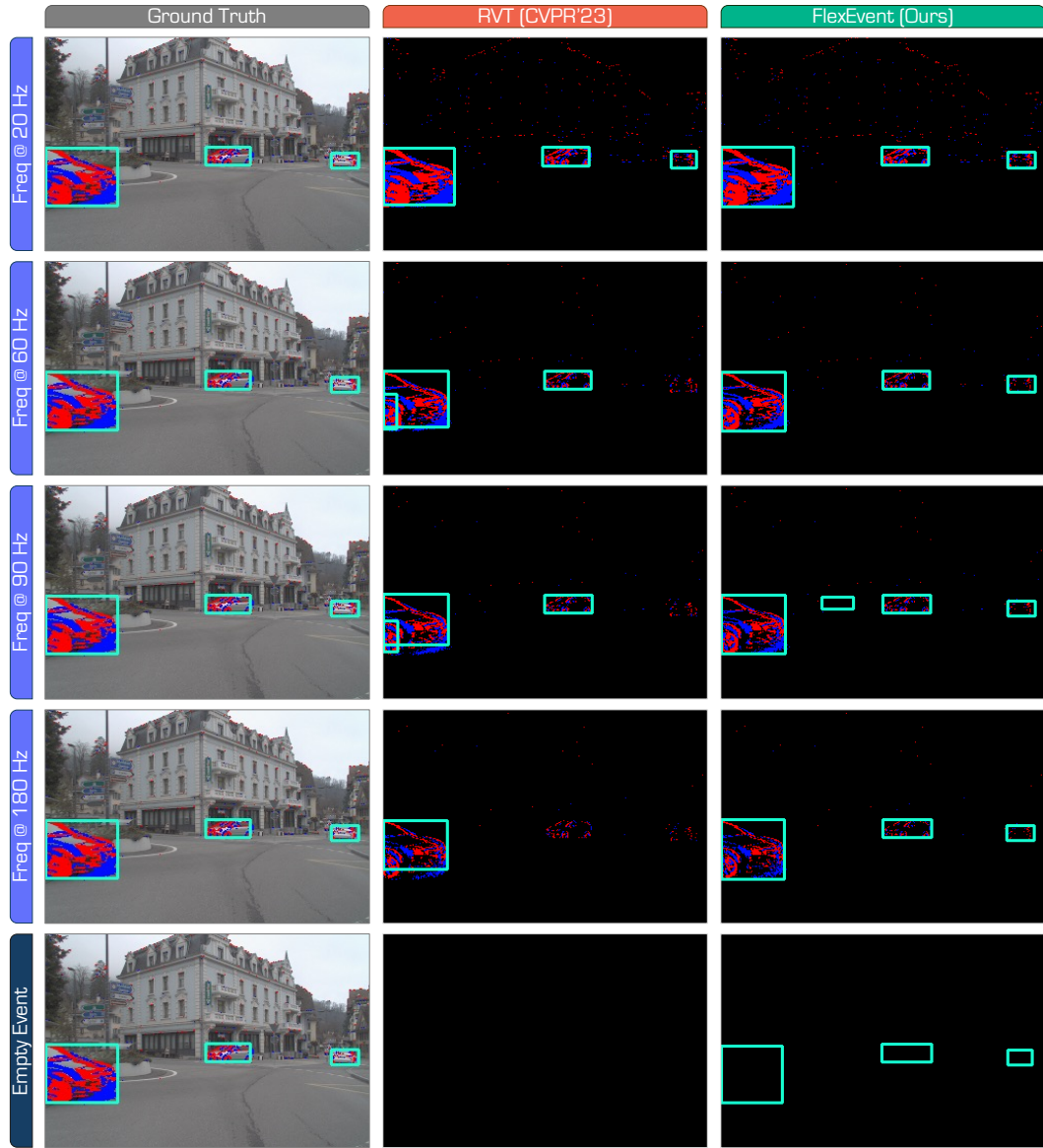


Figure 12: Additional qualitative comparisons of the RVT model (Gehrig & Scaramuzza, 2023) and the proposed **FlexEvent** under different event camera operation frequencies (20 Hz, 60 Hz, 90 Hz, and 180 Hz) and the empty event scenario. The experiments are conducted on the test set of *DSEC-Det*. Best viewed in colors.

## E PUBLIC RESOURCES USED

In this section, we acknowledge the public resources used, during the course of this work.

### E.1 PUBLIC DATASETS USED

- DSEC<sup>2</sup> ..... CC BY-SA 4.0
- DSEC-Det<sup>3</sup> ..... GNU General Public License v3.0
- DSEC-Detection<sup>4</sup> ..... Creative Commons Zero v1.0 Universal
- DSEC-MOD<sup>5</sup> ..... Unknown
- Gen 1<sup>6</sup> ..... Prophesee Gen1 Automotive Detection Dataset License
- 1 Mpx<sup>7</sup> ..... Prophesee 1Mpx Automotive Detection Dataset License

### E.2 PUBLIC IMPLEMENTATIONS USED

- RVT<sup>8</sup> ..... MIT License
- SAST<sup>9</sup> ..... MIT License
- SSM<sup>10</sup> ..... Unknown
- LEOD<sup>11</sup> ..... MIT License
- DAGr<sup>12</sup> ..... GNU General Public License v3.0
- RENet<sup>13</sup> ..... Unknown

---

<sup>2</sup><https://dsec.ifi.uzh.ch>

<sup>3</sup><https://github.com/uzh-rpg/dsec-det>

<sup>4</sup><https://github.com/abhishek1411/event-rgb-fusion>

<sup>5</sup><https://github.com/ZZY-Zhou/RENet>

<sup>6</sup><https://www.prophesee.ai/2020/01/24/prophesee-gen1-automotive-detection-dataset>

<sup>7</sup><https://www.prophesee.ai/2020/11/24/automotive-megapixel-event-based-dataset>

<sup>8</sup><https://github.com/uzh-rpg/RVT>

<sup>9</sup><https://github.com/Peterande/SAST>

<sup>10</sup>[https://github.com/uzh-rpg/ssms\\_event\\_cameras](https://github.com/uzh-rpg/ssms_event_cameras)

<sup>11</sup><https://github.com/Wuziyi616/LEOD>

<sup>12</sup><https://github.com/uzh-rpg/dagr>

<sup>13</sup><https://github.com/ZZY-Zhou/RENet>

## REFERENCES

- Hu Cao, Guang Chen, Jiahao Xia, Genghang Zhuang, and Alois Knoll. Fusion-based feature attention gate component for vehicle detection based on event camera. *IEEE Sensors Journal*, 21(21):24540–24548, 2021. [3](#) [8](#)
- Hu Cao, Guang Chen, Zhijun Li, Yingbai Hu, and Alois Knoll. Neurograsp: multimodal neural network with euler region regression for neuromorphic vision-based grasp pose estimation. *IEEE Transactions on Instrumentation and Measurement*, 71:1–11, 2022. [3](#)
- Hu Cao, Zehua Zhang, Yan Xia, Xinyi Li, Jiahao Xia, Guang Chen, and Alois Knoll. Embracing events and frames with hierarchical feature refinement network for object detection. In *European Conference on Computer Vision*, 2024. [3](#) [7](#) [8](#) [13](#)
- Guang Chen, Hu Cao, Canbo Ye, Zhenyan Zhang, Xingbo Liu, Xuhui Mo, Zhongnan Qu, Jörg Conradt, Florian Röhrbein, and Alois Knoll. Multi-cue event information fusion for pedestrian detection with neuromorphic vision sensors. *Frontiers in Neurorobotics*, 13:10, 2019. [3](#)
- Nicholas FY Chen. Pseudo-labels for supervised learning on dynamic vision sensor data, applied to object detection under ego-motion. In *IEEE/CVF Conference on Computer Vision and Pattern Recognition Workshops*, pp. 644–653, 2018. [3](#)
- Xiaokang Chen, Kwan-Yee Lin, Jingbo Wang, Wayne Wu, Chen Qian, Hongsheng Li, and Gang Zeng. Bi-directional cross-modality feature propagation with separation-and-aggregation gate for rgb-d semantic segmentation. In *European Conference on Computer Vision*, pp. 561–577, 2020. [8](#)
- Loïc Cordone, Benoît Miramond, and Philippe Thierion. Object detection with spiking neural networks on automotive event data. In *International Joint Conference on Neural Networks*, pp. 1–8, 2022. [2](#) [3](#)
- Javier Cuadrado, Ulysse Rançon, Benoit R. Cottereau, Francisco Barranco, and Timothée Masquelier. Optical flow estimation from event-based cameras and spiking neural networks. *Frontiers in Neuroscience*, 17:1160034, 2023. [3](#)
- Pierre De Tournemire, Davide Nitti, Etienne Perot, Davide Migliore, and Amos Sironi. A large scale event-based detection dataset for automotive. *arXiv preprint arXiv:2001.08499*, 2020. [4](#) [13](#)
- Tobias Fischer, Thomas E Huang, Jiangmiao Pang, Linlu Qiu, Haofeng Chen, Trevor Darrell, and Fisher Yu. Qdtrack: Quasi-dense similarity learning for appearance-only multiple object tracking. *IEEE Transactions on Pattern Analysis and Machine Intelligence*, 45(12):15380–15393, 2023. [12](#)
- Guillermo Gallego, Tobi Delbrück, Garrick Orchard, Chiara Bartolozzi, Brian Taba, Andrea Censi, Stefan Leutenegger, Andrew J. Davison, Jörg Conradt, Kostas Daniilidis, and Davide Scaramuzza. Event-based vision: A survey. *IEEE Transactions on Pattern Analysis and Machine Intelligence*, 44(1):154–180, 2022. [2](#)
- Daniel Gehrig and Davide Scaramuzza. Pushing the limits of asynchronous graph-based object detection with event cameras. *arXiv preprint arXiv:2211.12324*, 2022. [2](#) [3](#)
- Daniel Gehrig and Davide Scaramuzza. Low-latency automotive vision with event cameras. *Nature*, 629(8014):1034–1040, 2024. [2](#) [3](#) [7](#) [8](#) [9](#) [10](#) [12](#) [13](#) [15](#) [16](#) [17](#) [19](#) [20](#) [21](#)
- Daniel Gehrig, Henri Rebecq, Guillermo Gallego, and Davide Scaramuzza. Eklt: Asynchronous photometric feature tracking using events and frames. *International Journal of Computer Vision*, 128(3):601–618, 2020. [3](#)
- Daniel Gehrig, Michelle Rüegg, Mathias Gehrig, Javier Hidalgo-Carrió, and Davide Scaramuzza. Combining events and frames using recurrent asynchronous multimodal networks for monocular depth prediction. *IEEE Robotics and Automation Letters*, 6(2):2822–2829, 2021a. [3](#) [8](#)
- Mathias Gehrig and Davide Scaramuzza. Recurrent vision transformers for object detection with event cameras. In *IEEE/CVF Conference on Computer Vision and Pattern Recognition*, pp. 13884–13893, 2023. [1](#) [3](#) [5](#) [7](#) [9](#) [10](#) [13](#) [14](#) [19](#) [20](#) [21](#) [22](#) [23](#) [24](#)

- Mathias Gehrig, Willem Aarents, Daniel Gehrig, and Davide Scaramuzza. Dsec: A stereo event camera dataset for driving scenarios. *IEEE Robotics and Automation Letters*, 6(3):4947–4954, 2021b. [2](#), [12](#)
- Kaiming He, Xiangyu Zhang, Shaoqing Ren, and Jian Sun. Deep residual learning for image recognition. In *IEEE/CVF Conference on Computer Vision and Pattern Recognition*, pp. 770–778, 2016. [5](#)
- Jie Hu, Li Shen, and Gang Sun. Squeeze-and-excitation networks. In *IEEE/CVF Conference on Computer Vision and Pattern Recognition*, pp. 7132–7141, 2018. [8](#)
- Massimiliano Iacono, Stefan Weber, Arren Glover, and Chiara Bartolozzi. Towards event-driven object detection with off-the-shelf deep learning. In *IEEE/RSJ International Conference on Intelligent Robots and Systems*, pp. 1–9, 2018. [3](#)
- Kamil Jeziorek, Andrea Pinna, and Tomasz Kryjak. Memory-efficient graph convolutional networks for object classification and detection with event cameras. In *Signal Processing: Algorithms, Architectures, Arrangements, and Applications*, pp. 160–165, 2023. [2](#)
- Wei Ji, Jingjing Li, Shuang Yu, Miao Zhang, Yongri Piao, Shunyu Yao, Qi Bi, Kai Ma, Yefeng Zheng, Huchuan Lu, et al. Calibrated rgb-d salient object detection. In *IEEE/CVF Conference on Computer Vision and Pattern Recognition*, pp. 9471–9481, 2021. [8](#)
- Zhuangyi Jiang, Pengfei Xia, Kai Huang, Walter Stechele, Guang Chen, Zhenshan Bing, and Alois Knoll. Mixed frame-/event-driven fast pedestrian detection. In *IEEE International Conference on Robotics and Automation*, pp. 8332–8338, 2019. [3](#)
- Glenn Jocher. Ultralytics yolov5, 2020. URL <https://github.com/ultralytics/yolov5>. [12](#)
- Diederik P Kingma. Adam: A method for stochastic optimization. *arXiv preprint arXiv:1412.6980*, 2014. [14](#)
- Simon Klenk, David Bonello, Lukas Koestler, and Daniel Cremers. Masked event modeling: Self-supervised pretraining for event cameras. *arXiv preprint arXiv:2212.10368*, 2022. [3](#)
- Lingdong Kong, Youquan Liu, Lai Xing Ng, Benoit R. Cottereau, and Wei Tsang Ooi. Openess: Event-based semantic scene understanding with open vocabularies. In *IEEE/CVF Conference on Computer Vision and Pattern Recognition*, pp. 15686–15698, 2024. [3](#)
- Dianze Li, Yonghong Tian, and Jianing Li. Sodformer: Streaming object detection with transformer using events and frames. *IEEE Transactions on Pattern Analysis and Machine Intelligence*, 45(11):14020–14037, 2023. [3](#)
- Jianing Li, Siwei Dong, Zhaofei Yu, Yonghong Tian, and Tiejun Huang. Event-based vision enhanced: A joint detection framework in autonomous driving. In *IEEE International Conference on Multimedia and Expo*, pp. 1396–1401, 2019. [3](#)
- Jianing Li, Jia Li, Lin Zhu, Xijie Xiang, Tiejun Huang, and Yonghong Tian. Asynchronous spatio-temporal memory network for continuous event-based object detection. *IEEE Transactions on Image Processing*, 31:2975–2987, 2022. [3](#)
- Tsung-Yi Lin, Michael Maire, Serge Belongie, James Hays, Pietro Perona, Deva Ramanan, Piotr Dollár, and C Lawrence Zitnick. Microsoft coco: Common objects in context. In *European Conference on Computer Vision*, pp. 740–755, 2014. [7](#), [13](#)
- Nico Messikommer, Daniel Gehrig, Antonio Loquercio, and Davide Scaramuzza. Event-based asynchronous sparse convolutional networks. In *European Conference on Computer Vision*, pp. 415–431, 2020. [2](#), [3](#)
- Farzeen Munir, Shoaib Azam, Kin-Choong Yow, Byung-Geun Lee, and Moongu Jeon. Multimodal fusion for sensorimotor control in steering angle prediction. *Engineering Applications of Artificial Intelligence*, 126:107087, 2023. [8](#)

- Jiangmiao Pang, Linlu Qiu, Xia Li, Haofeng Chen, Qi Li, Trevor Darrell, and Fisher Yu. Quasi-dense similarity learning for multiple object tracking. In *IEEE/CVF Conference on Computer Vision and Pattern Recognition*, pp. 164–173, 2021. [12](#)
- Yansong Peng, Hebei Li, Yueyi Zhang, Xiaoyan Sun, and Feng Wu. Scene adaptive sparse transformer for event-based object detection. In *IEEE/CVF Conference on Computer Vision and Pattern Recognition*, pp. 16794–16804, 2024. [3](#), [7](#), [9](#), [13](#), [19](#), [20](#), [21](#)
- Etienne Perot, Pierre De Tournemire, Davide Nitti, Jonathan Masci, and Amos Sironi. Learning to detect objects with a 1 megapixel event camera. *Advances in Neural Information Processing Systems*, 33:16639–16652, 2020. [2](#), [3](#), [4](#), [13](#)
- Henri Rebecq, René Ranftl, Vladlen Koltun, and Davide Scaramuzza. Events-to-video: Bringing modern computer vision to event cameras. In *IEEE/CVF Conference on Computer Vision and Pattern Recognition*, pp. 3857–3866, 2019. [3](#)
- Henri Rebecq, René Ranftl, Vladlen Koltun, and Davide Scaramuzza. High speed and high dynamic range video with an event camera. *IEEE Transactions on Pattern Analysis and Machine Intelligence*, 43(6):1964–1980, 2021. [3](#)
- Simon Schaefer, Daniel Gehrig, and Davide Scaramuzza. Aegnn: Asynchronous event-based graph neural networks. In *IEEE/CVF Conference on Computer Vision and Pattern Recognition*, pp. 12371–12381, 2022. [2](#), [3](#)
- Leslie N Smith and Nicholay Topin. Super-convergence: Very fast training of neural networks using large learning rates. In *Artificial Intelligence and Machine Learning for Multi-Domain Operations Applications*, volume 11006, pp. 369–386, 2019. [14](#)
- Lea Steffen, Daniel Reichard, Jakob Weinland, Jacques Kaiser, Arne Roennau, and Rüdiger Dillmann. Neuromorphic stereo vision: A survey of bio-inspired sensors and algorithms. *Frontiers in Neuroscience*, 13:28, 2019. [2](#)
- Timo Stoffregen, Cedric Scheerlinck, Davide Scaramuzza, Tom Drummond, Nick Barnes, Lindsay Kleeman, and Robert Mahony. Reducing the sim-to-real gap for event cameras. In *European Conference on Computer Vision*, pp. 534–549, 2020. [3](#)
- Daobo Sun and Haibo Ji. Event-based object detection using graph neural networks. In *IEEE Conference on Data Driven Control and Learning Systems*, pp. 1895–1900, 2023. [3](#)
- Lei Sun, Christos Sakaridis, Jingyun Liang, Qi Jiang, Kailun Yang, Peng Sun, Yaozu Ye, Kaiwei Wang, and Luc Van Gool. Event-based fusion for motion deblurring with cross-modal attention. In *European Conference on Computer Vision*, pp. 412–428, 2022a. [3](#), [4](#), [8](#)
- Zhaoning Sun, Nico Messikommer, Daniel Gehrig, and Davide Scaramuzza. Ess: Learning event-based semantic segmentation from still images. In *European Conference on Computer Vision*, pp. 341–357, 2022b. [3](#)
- Abhishek Tomy, Anshul Paigwar, Khushdeep S Mann, Alessandro Renzaglia, and Christian Laugier. Fusing event-based and rgb camera for robust object detection in adverse conditions. In *IEEE International Conference on Robotics and Automation*, pp. 933–939, 2022. [2](#), [3](#), [7](#), [8](#), [12](#)
- SM Nadim Uddin, Soikat Hasan Ahmed, and Yong Ju Jung. Unsupervised deep event stereo for depth estimation. *IEEE Transactions on Circuits and Systems for Video Technology*, 32(11):7489–7504, 2022. [3](#)
- Lin Wang, Yujeong Chae, Sung-Hoon Yoon, Tae-Kyun Kim, and Kuk-Jin Yoon. Evdistill: Asynchronous events to end-task learning via bidirectional reconstruction-guided cross-modal knowledge distillation. In *IEEE/CVF Conference on Computer Vision and Pattern Recognition*, pp. 608–619, 2021. [3](#)
- Qilong Wang, Banggu Wu, Pengfei Zhu, Peihua Li, Wangmeng Zuo, and Qinghua Hu. Eca-net: Efficient channel attention for deep convolutional neural networks. In *IEEE/CVF Conference on Computer Vision and Pattern Recognition*, pp. 11534–11542, 2020. [8](#)

- Sanghyun Woo, Jongchan Park, Joon-Young Lee, and In So Kweon. Cbam: Convolutional block attention module. In *European Conference on Computer Vision*, pp. 3–19, 2018. [8](#)
- Ziyi Wu, Xudong Liu, and Igor Gilitschenski. Eventclip: Adapting clip for event-based object recognition. *arXiv preprint arXiv:2306.06354*, 2023. [3](#)
- Ziyi Wu, Mathias Gehrig, Qing Lyu, Xudong Liu, and Igor Gilitschenski. Leod: Label-efficient object detection for event cameras. In *IEEE/CVF Conference on Computer Vision and Pattern Recognition*, pp. 16933–16943, 2024. [3, 7, 13](#)
- Yan Yang, Liyuan Pan, and Liu Liu. Event camera data pre-training. In *IEEE/CVF International Conference on Computer Vision*, pp. 10699–10709, 2023. [3](#)
- Jiaming Zhang, Huayao Liu, Kailun Yang, Xinxin Hu, Ruiping Liu, and Rainer Stiefelhagen. Cmx: Cross-modal fusion for rgb-x semantic segmentation with transformers. *IEEE Transactions on Intelligent Transportation Systems*, 24(12):14679–14694, 2023. [8](#)
- Jiqing Zhang, Bo Dong, Haiwei Zhang, Jianchuan Ding, Felix Heide, Baocai Yin, and Xin Yang. Spiking transformers for event-based single object tracking. In *IEEE/CVF Conference on Computer Vision and Pattern Recognition*, pp. 8801–8810, 2022. [3](#)
- Limeng Zhang, Hongguang Zhang, Jihua Chen, and Lei Wang. Hybrid deblur net: Deep non-uniform deblurring with event camera. *IEEE Access*, 8:148075–148083, 2020. [3](#)
- Jiang Zhao, Shilong Ji, Zhihao Cai, Yiwen Zeng, and Yingxun Wang. Moving object detection and tracking by event frame from neuromorphic vision sensors. *Biomimetics*, 7(1):31, 2022. [3](#)
- Ge Zheng, Liu Songtao, Wang Feng, Li Zeming, and Sun Jian. Yolox: Exceeding yolo series in 2021. *arXiv preprint arXiv:2107.08430*, 2021. [7, 14](#)
- Zihan Zhong, Zhiqiang Tang, Tong He, Haoyang Fang, and Chun Yuan. Convolution meets lora: Parameter efficient finetuning for segment anything model. *arXiv preprint arXiv:2401.17868*, 2024. [5](#)
- Tao Zhou, Huazhu Fu, Geng Chen, Yi Zhou, Deng-Ping Fan, and Ling Shao. Specificity-preserving rgb-d saliency detection. In *Proceedings of the IEEE/CVF international conference on computer vision*, pp. 4681–4691, 2021. [8](#)
- Zhuyun Zhou, Zongwei Wu, Rémi Boutteau, Fan Yang, Cédric Demonceaux, and Dominique Ginhac. Rgb-event fusion for moving object detection in autonomous driving. In *IEEE International Conference on Robotics and Automation*, pp. 7808–7815, 2023. [2, 3, 5, 7, 8, 12, 13](#)
- Alex Zihao Zhu, Liangzhe Yuan, Kenneth Chaney, and Kostas Daniilidis. Unsupervised event-based learning of optical flow, depth, and egomotion. In *IEEE/CVF Conference on Computer Vision and Pattern Recognition*, 2019. [3](#)
- Xiao-Long Zou, Tie-Jun Huang, and Si Wu. Towards a new paradigm for brain-inspired computer vision. *Machine Intelligence Research*, 19(5):412–424, 2022. [2](#)
- Nikola Zubić, Daniel Gehrig, Mathias Gehrig, and Davide Scaramuzza. From chaos comes order: Ordering event representations for object recognition and detection. In *IEEE/CVF International Conference on Computer Vision*, pp. 12846–12856, 2023. [3](#)
- Nikola Zubić, Mathias Gehrig, and Davide Scaramuzza. State space models for event cameras. In *IEEE/CVF Conference on Computer Vision and Pattern Recognition*, pp. 5819–5828, 2024. [3, 7, 13](#)